BIOPROBES 81

JOURNAL OF CELL BIOLOGY APPLICATIONS SUMMER 2020

3D midbrain model using neural organoids

Floor plate differentiation of dopaminergic neurons in 3D culture

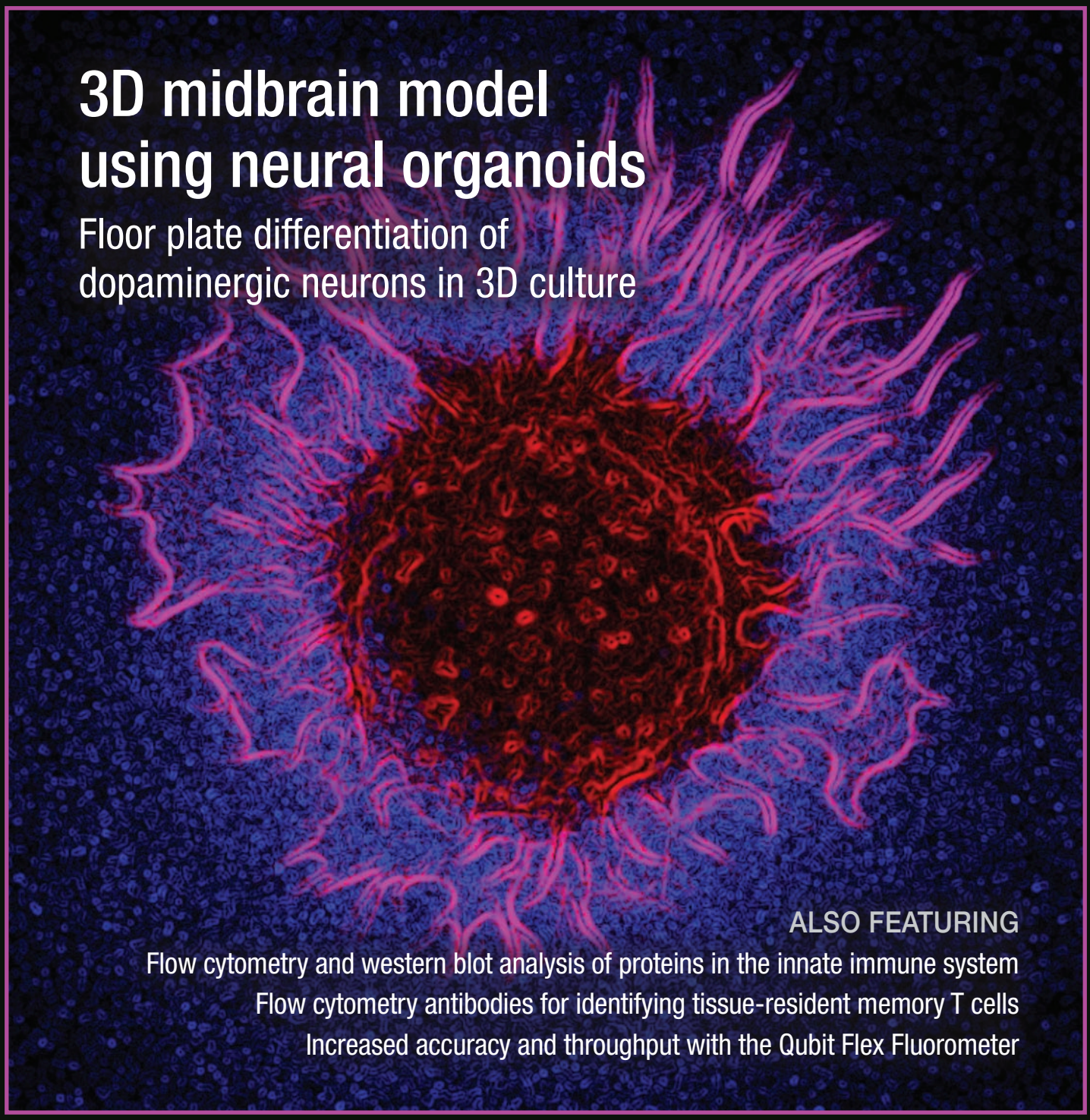

ALSO FEATURING

Flow cytometry and western blot analysis of proteins in the innate immune system

Flow cytometry antibodies for identifying tissue-resident memory T cells

Increased accuracy and throughput with the Qubit Flex Fluorometer

ThermoFisher SCIENTIFIC

BioProbes 81

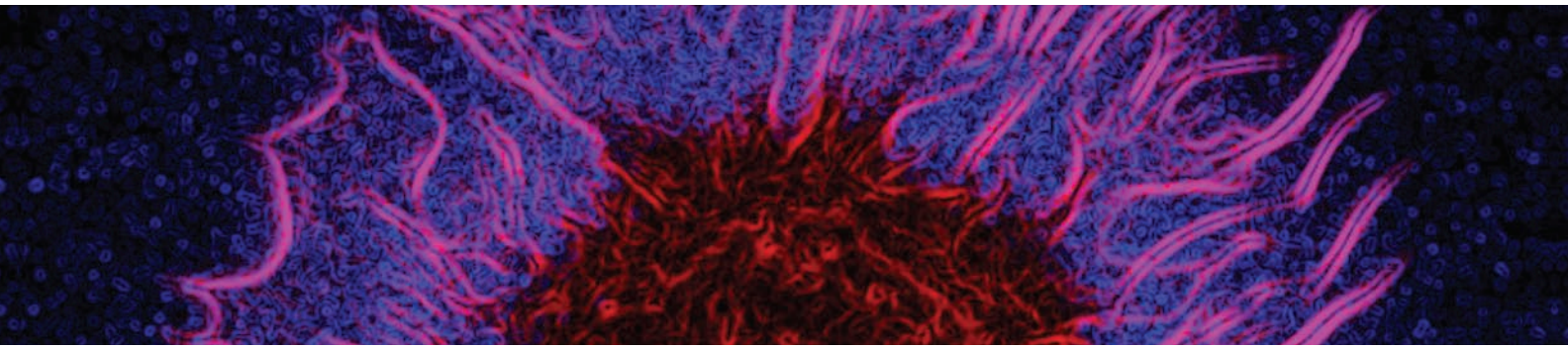

thermofisher.com/bioprobes • Summer 2020

Production Manager
Beth Browne

Editors
Michelle Spence
Deborah Bright
Kevin Kepple
Grace Richter

Designer
Kim McGovern

Authors and Reviewers
Brian Almond
Jolene Bradford
Christine Brotski
Beth Browne
Suzanne Buck
Shelley Das
Melanie Dowd
Sarvani Emani
Adyary Fallarero
Helen Fleisig
Debra Gale
Kamran Jamil
Richard Josephson
William Kang
Chris Langsdorf
Shekar Menon
Leticia Montoya
Adam Pelzek
Carla Potts
Sneh Ringwala
Tomas Roa-Lauby
Matt Schifano
Thao Sebata
Jessica Slack
Eliza Small
Cameron Smurthwaite
Tina Song
Haripriya Sridharan
Priyanka Swamynathan

BioProbes Journal, available in print and online at **thermofisher.com/bioprobes**, is dedicated to providing researchers with the very latest information about cell biology products and their applications. For a complete list of our products, along with extensive descriptions and literature references, please see our website.

Subscribe to *BioProbes Journal* at thermofisher.com/subscribebp

More choices with new antibodies from selected suppliers

Target-specific antibodies are critical reagents in today's cutting-edge research, driving the need for more choices. We are partnering with selected antibody vendors to provide you online access to more primary antibodies from multiple companies at **thermofisher.com/antibodies**.

To easily find what you need, utilize the enhanced online search tool to search, compare, and purchase antibodies from our expansive portfolio. Start by typing in the protein target to find the most relevant options, and then use filters to narrow the search. You can explore relevant and detailed information such as published figures, advanced verification data, references, images, and citations. Compare these key product features to help you make your decision. Additional useful tools include the ability to create and share lists with colleagues or request custom or bulk orders. Get started today at **thermofisher.com/antibodies**.

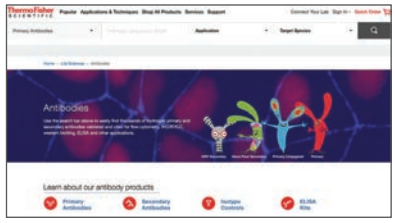

On-demand webinar: Strategies for isolation of plasma membrane proteins

Isolating plasma membrane proteins presents many challenges, and it can often prove difficult to choose the right method based on the sample and downstream application. This webinar focuses on robust and optimized techniques for extraction, isolation, and enrichment of cell-surface proteins, including stable and functional G protein–coupled receptors (GPCRs). In this webinar, we present:

- Techniques for isolating plasma membrane proteins
- Ways to produce stable and functional GPCR extracts
- Enrichment methods for cell-surface proteins that produce minimal off-target contaminants and have been verified using mass spectrometry
- How cell-surface proteins can serve as a treasure trove of pharma-relevant targets for potential drug therapy

View this webinar at **thermofisher.com/membraneprotein**.

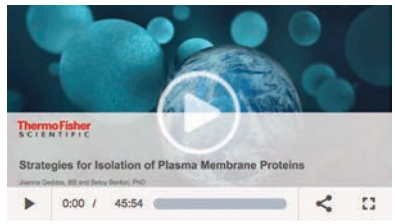

Updated: The Attune NxT Flow Cytometer reference article database

Scientists at Thermo Fisher Scientific have established a reference article database that features over 475 peer-reviewed publications citing the use of the Invitrogen™ Attune™ NxT Flow Cytometer. You can easily perform keyword searches (e.g., author, cell type, species) to access hundreds of articles in various areas of life science research, from immunology, immunotherapy, cancer, and drug discovery, to food, agriculture, and veterinary and materials sciences. It includes scientific articles published through 2019, and we are committed to updating it with new references as they are published. Learn more about how the Attune NxT Flow Cytometer can enhance your research with its ability to provide consistent results, whether samples are dilute or concentrated, require fast or slow flow rates, or are susceptible to clogging during analysis. To explore the Attune NxT reference database, go to **thermofisher.com/attunenxtarticles**.

Species representation in the Attune NxT reference database

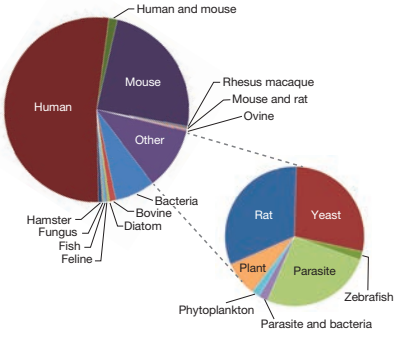

Behind the Bench blog: The latest antibody news

We are continually updating our Invitrogen™ antibody portfolio with validated* primary antibodies for use in flow cytometry, IF/ICC/IHC, western blotting, and ELISAs. Check out these recent blog posts, showcasing the latest antibody data for selected nucleic acid and protein research topics:

- Translate to Invitrogen antibodies for your ribosomal protein research!
- Drivers of the chromosomal passenger complex
- Pairing Invitrogen ChIP-validated* antibodies with your DNA repair protein research

Find these posts and more at **thermofisher.com/blog/behindthebench**. Learn about our validation methods at **thermofisher.com/antibodyvalidation**. Or, go directly to our antibody search tool at **thermofisher.com/antibodies**.

*The use or any variation of the word "validation" refers only to research use antibodies that were subject to functional testing to confirm that the antibody can be used with the research techniques indicated. It does not ensure that the product(s) was validated for clinical or diagnostic uses.

Introducing BlotBuilder: A new western blot product selection tool

Imagine if you could obtain a personalized western blot solution designed specifically for your experimental needs—in just 2 minutes. Now you can with our new Invitrogen™ BlotBuilder™ Western Blot Product Selection Tool, which can help you quickly and easily find the optimal set of western blot products for detection of your protein. Simply answer 5 questions and get a customized western blot protocol and product list based on your needs. Customize your western blot experience today with our BlotBuilder tool at **thermofisher.com/blotbuilder**.

Best practices: 5 steps to intracellular flow cytometry

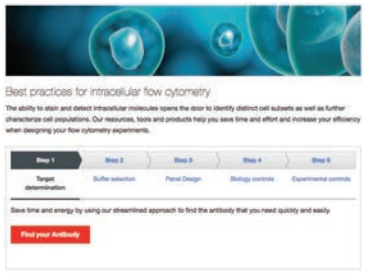

The ability to detect intracellular proteins with flow cytometry opens the door to a more complete characterization of cell populations and distinct subsets within those populations. To help you save time and effort and increase your efficiency when designing flow cytometry experiments, we have organized our resources, tools, and products for intracellular flow cytometry into 5 simple steps:

- **Step 1:** Target determination, with a link to our antibody search tool
- **Step 2:** Buffer selection, with fixation and permeabilization buffers for cytoplasmic and nuclear staining
- **Step 3:** Panel design, with online tools to create a customized panel and search published multicolor flow cytometry panels
- **Step 4:** Biological controls, with a product selection guide that contains fluorescent cell stains for removing dead cells and unwanted artifacts from your analysis
- **Step 5:** Experimental controls, with products to facilitate antibody compensation controls

Access the "5 steps to intracellular flow cytometry" web page at **thermofisher.com/5steps-icfc**.

SlowFade Glass Antifade Mountants: Unparalleled focal depth

Obtain the sharpest deep-tissue images with Invitrogen™ SlowFade™ Glass Soft-Set Antifade Mountant, which features a refractive index of 1.52 (similar to glass coverslips) and provides superior photobleaching protection. This noncuring mountant is compatible with oil-immersion microscope optics and enables a refraction-free light path and minimized spherical aberration, which improves axial resolution threefold (at 150 µm focal depth) as measured by point spread function. When 1 mm–thick tissue sections are mounted in SlowFade Glass Soft-Set Antifade Mountant, there is visible optical tissue clearing, enabling deep-tissue 3D imaging. Learn more about our growing portfolio of noncuring and hard-set antifade mountants, now available with Invitrogen™ DAPI or SYTOX™ Deep Red counterstains, at **thermofisher.com/antifade**.

Product	Quantity	Cat. No.
SlowFade™ Glass Soft-Set Antifade Mountant	2 mL	S36917
	10 mL	S36918
	5 x 2 mL	S36916
SlowFade™ Glass Soft-Set Antifade Mountant, with DAPI	2 mL	S36920
	10 mL	S36921
	5 x 2 mL	S36919

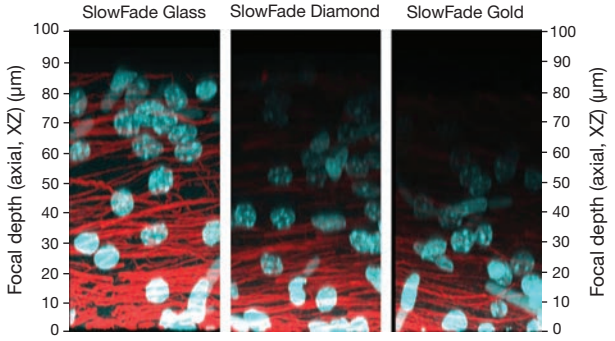

Unparalleled focal depth in 100 µm–thick brain tissue sections with SlowFade Glass Soft-Set Antifade Mountant. Cryopreserved 100 µm–thick rat brain sections were stained for GFAP (red) with Invitrogen™ GFAP rabbit primary antibody (Cat. No. OPA1-06100) and Invitrogen™ Alexa Fluor™ Plus 594 goat anti–rabbit IgG secondary antibody (Cat. No. A32740) overnight. Nuclei (cyan) were stained with Invitrogen™ DAPI nuclear stain (Cat. No. D1306). Stained tissue sections were mounted with Invitrogen™ SlowFade™ Glass Soft-Set (Cat. No. S36917), SlowFade™ Diamond (Cat. No. S36967), or SlowFade™ Gold (Cat. No. S36940) Antifade Mountant and imaged on a Zeiss™ LSM 710 confocal microscope.

Alexa Fluor Phalloidins for superior actin cytoskeleton imaging

Invitrogen™ Alexa Fluor™ Plus 555 and Alexa Fluor™ Plus 647 Phalloidins are high-affinity F-actin probes conjugated to our bright and photostable Alexa Fluor Plus dyes. These phalloidin conjugates are specially designed to produce the maximum density of both phalloidin and Alexa Fluor Plus dye molecules on an F-actin filament, resulting in 3 to 5 times more fluorescent signal for superior actin cytoskeleton imaging.

The probes are designed to produce excellent sensitivity and specificity when visualizing and quantifying F-actin in cells, tissue sections, or cell-free preparations. Their extra brightness is especially useful when conducting challenging F-actin imaging, such as structured illumination microscopy (SIM) or stochastic optical reconstruction microscopy (STORM), or for reliable staining of stress fibers. Phalloidin-based actin staining is fully compatible with other fluorescent stains used in cell analyses. Learn more at **thermofisher.com/phalloidin**.

Product	Quantity	No. of slides	Cat. No.
Alexa Fluor™ Plus 555 Phalloidin	1 each	300	A30106
Alexa Fluor™ Plus 647 Phalloidin	1 each	300	A30107

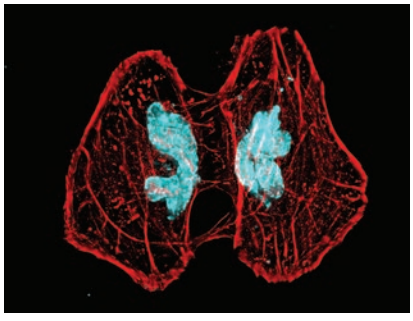

Multicolor fluorescence imaging of stained HeLa cells. HeLa cells were stained with Invitrogen™ Alexa Fluor™ Plus 555 Phalloidin (Cat. No. A30106) and Invitrogen™ NucBlue™ Live ReadyProbes™ Reagent (Cat. No. R37605), mounted in Invitrogen™ ProLong™ Glass Antifade Mountant (Cat. No. P36984), and imaged using the Invitrogen™ EVOS™ M7000 Imaging System (Cat. No. AMF7000) with an Olympus™ 60x apochromat oil objective (Cat. No. AMEP4694) and Invitrogen™ EVOS™ DAPI (Cat. No. AMEP4650) and RFP (Cat. No. AMEP4652) light cubes.

CountBright Plus beads: Absolute cell counting with greater accuracy and ease

Absolute cell counting beads are widely used in flow cytometry experiments to quantify cell populations and study disease progression. They can also be used to validate flow cytometric absolute cell counting results. Compared with the original Invitrogen™ CountBright™ Absolute Counting Beads, the new Invitrogen™ CountBright™ Plus beads offer: (1) a greater percentage of singlets for improved accuracy and consistency, and (2) excitation by a wider range of wavelengths, from ultraviolet (350 nm) to infrared (808 nm), with emissions between 385 and 860 nm. The CountBright Plus beads also have a 4 µm diameter, which is similar to that of blood cells and enables cell counting beads to be on scale for FSC/SSC graphs. Find out more about our selection of flow cytometry cell counting beads at **thermofisher.com/countbrightplus**.

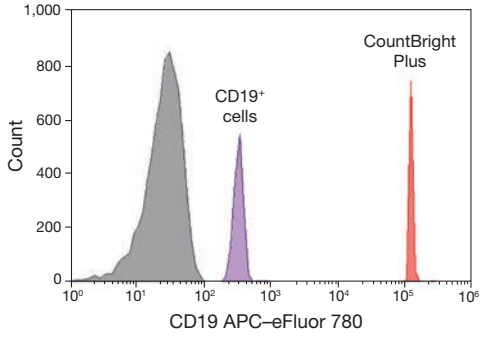

Simultaneous detection of CountBright Plus Absolute Counting Beads and near-IR–emitting fluorophores. Invitrogen™ CountBright™ Plus Absolute Counting Beads (Cat. No. C36995) are detected simultaneously with Invitrogen™ APC–eFluor™ 780 CD19 antibody–stained cells in lysed whole blood excited with an infrared laser.

Product	Quantity	Cat. No.
CountBright™ Plus Absolute Counting Beads	100 tests	C36995

TMTpro 16plex Isobaric Label Reagents: Next-generation tandem mass tags

Thermo Scientific™ TMTpro™ 16plex Isobaric Label Reagents represent the next generation of tandem mass tags for mass spectrometry. They are designed to increase the level of sample multiplexing without compromising either protein identification or quantitation. These new TMTpro label reagents have the same labeling efficiency and peptide/protein ID rates and are similar in design to the original Thermo Scientific™ TMT™ label reagents (i.e., they are both isobaric and amine-reactive); however, they differ in structure, with a longer spacer region and an isobutyl proline mass reporter region.

The higher multiplex capability provided by the TMTpro label reagents results in fewer missing quantitative values among samples and within replicates. These new tandem mass tags are designed to produce superior quantitative accuracy and precision. Find out more about our selection of tandem mass tag systems at **thermofisher.com/tmtpro**.

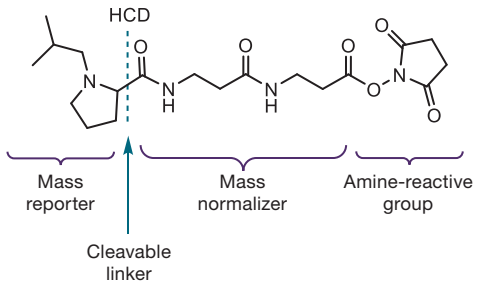

The general chemical structure of the TMTpro isobaric label reagents.

Product	Quantity	Cat. No.
TMTpro™ 16plex Label Reagent Set (sufficient for one 16plex isobaric experiment)	1 x 0.5 mg (per tag)	A44521
TMTpro™ 16plex Label Reagent Set (sufficient for six 16plex isobaric experiments)	6 x 0.5 mg (per tag)	A44522
TMTpro™ 16plex Label Reagent Set (sufficient for ten 16plex isobaric experiments)	1 x 5 mg (per tag)	A44520
TMTpro™ Zero Label Reagent (sufficient for labeling five samples)	5 x 0.5 mg	A44519
TMTpro™ Zero Label Reagent (sufficient for labeling ten samples)	1 x 5 mg	A44518

ProcartaPlex multiplex immunoassay panels for neuroscience research

Invitrogen™ ProcartaPlex™ multiplex immunoassay panels offer the ability to measure and track multiple biomarkers over time for a variety of conditions of the central nervous system (CNS)—including brain trauma, stroke, multiple sclerosis, and Parkinson's and Alzheimer's disease—that can trigger neuroinflammation and dysfunction of the blood–brain barrier. This dysfunction can result in an increase in the concentrations of brain-specific molecules in circulation. Evaluation of the concentrations of these molecules in accessible biofluids, such as cerebrospinal fluid or blood, using the ProcartaPlex neuroscience immunoassay panels for the Luminex® xMAP® instrument platform may help with the identification and monitoring of the inflammatory response and progression of neurodegenerative disease. Find out more at **thermofisher.com/neuroprocartaplex**.

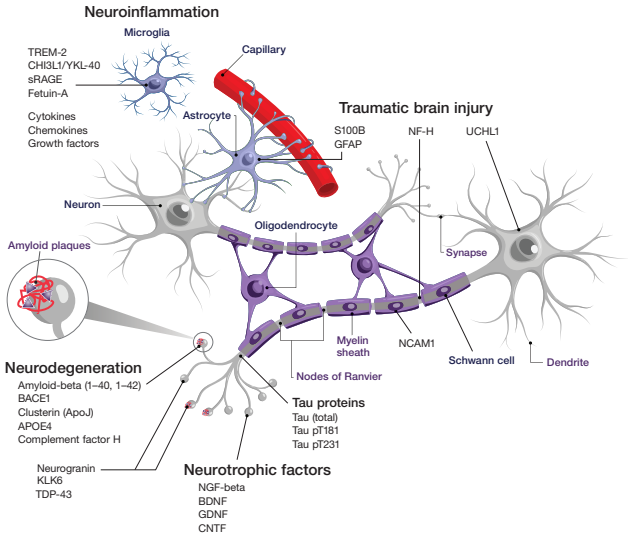

Elements of the central nervous system. The Invitrogen™ Neuroscience 18-plex Human ProcartaPlex™ Panel can be used to simultaneously measure 18 different markers in biofluids such as cerebrospinal fluid or blood that play a role in neuroinflammation, neurodegeneration, and traumatic brain injury.

Product	Cat. No.
Neuroscience 18-plex Human ProcartaPlex™ Panel	EPX180-15837-901
Neurodegeneration 9-plex Human ProcartaPlex™ Panel 1	EPX090-15836-901
Neurodegeneration 4-plex Human ProcartaPlex™ Panel 2	EPX040-15832-901
Brain Injury 5-plex Human ProcartaPlex™ Panel	EPX050-15838-901
Neurotrophic Factors 4-plex Human ProcartaPlex™ Panel	EPX040-15828-901
Neuroinflammation 6-plex Human ProcartaPlex™ Panel	EPX060-15833-901

ProQuantum high-sensitivity immunoassays: Now over 60 available targets

The Invitrogen™ ProQuantum™ high-sensitivity immunoassay kits offer affordable, ready-to-use, qPCR-based protein quantitation that consume as little as 2 µL of sample for triplicate data (a typical ELISA requires 150 µL). The assay protocol is streamlined with no wash steps, a single 1-hour incubation, and results in only 2 hours. With qPCR amplification, this immunoassay provides a very broad dynamic range (≥5 orders of magnitude) and high sensitivity, giving you the best chances of detecting the protein of interest. For more information and to see all available targets, go to **thermofisher.com/proquantum**.

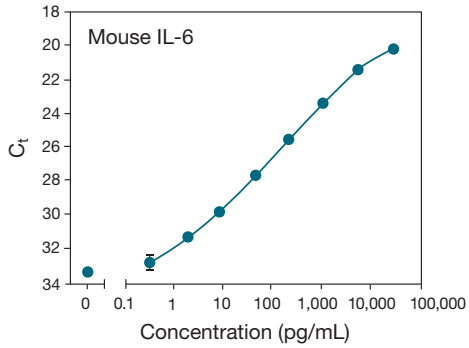

Standard curve for the ProQuantum Mouse IL-6 Immunoassay Kit. This standard curve, obtained using the Invitrogen™ ProQuantum™ Mouse IL-6 Immunoassay Kit (Cat. No. A43656), shows an assay range of 0.32–25,000 pg/mL.

Product	Quantity	Cat. No.
ProQuantum™ Mouse IFNγ Immunoassay Kit	96 tests	A41150
ProQuantum™ Mouse IL-6 Immunoassay Kit	96 tests	A43656
ProQuantum™ Mouse IL-17A Immunoassay Kit	96 tests	A46737
ProQuantum™ Mouse TNFα Immunoassay Kit	96 tests	A43658
ProQuantum™ Mouse VEGF Immunoassay Kit	96 tests	A46562

Innovative chemistry in the new Click-iT EdU Proliferation Assay for Microplates

Measuring mammalian cell proliferation is a fundamental method for assessing cell health, determining genotoxicity, and evaluating anti-cancer drugs. The new-and-improved Invitrogen™ Click-iT™ EdU Proliferation Assay for Microplates directly detects and quantifies DNA synthesis using a simplified and robust method that relies on click chemistry.

After EdU (a modified thymidine analog) is incorporated into newly synthesized DNA, a horseradish peroxidase (HRP) azide derivative is covalently attached to the incorporated EdU via a highly specific click reaction. The Invitrogen™ Amplex™ UltraRed Reagent, an HRP substrate included in this kit, is then added and the resulting fluorescence signal detected. Because of the highly specific attachment of HRP to EdU, the assay provides a highly sensitive and reliable measurement of mammalian cell proliferation in a microplate format. Furthermore, compared with the previous version of this assay, the new Click-iT EdU Proliferation Assay for Microplates shows very significant increases in sensitivity and assay dynamic range. For more information on our full range of assay kits and labeling reagents that utilize Click-iT technology, go to **thermofisher.com/clickitedu**.

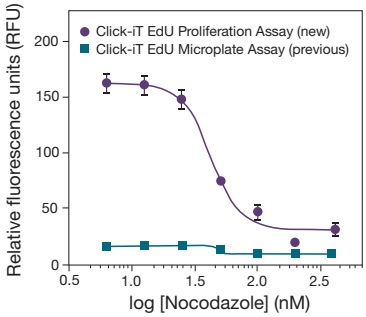

Significant performance improvement demonstrated using the new Click-iT EdU Proliferation Assay for Microplates. HeLa cells were seeded into 96-well plates, incubated overnight to allow for attachment, and then treated with various concentrations of nocodazole, which interferes with microtubule polymerization leading to an arrest of mitosis. After drug treatment, EdU was added, the cells were incubated for 2 hr, and cell proliferation was detected using the previous version (Cat. No. C10214, now discontinued) and the new version (Cat. No. C10499) of the Invitrogen™ Click-iT™ EdU Proliferation Assay for Microplates.

Product	Quantity	Cat. No.
Click-iT™ EdU Proliferation Assay for Microplates	400 assays	C10499

SiteClick Antibody Labeling Kits: Now available in large pack sizes

The Invitrogen™ SiteClick™ Antibody Labeling Kits, which produce labeled primary antibodies using highly efficient, site-specific, click labeling chemistry, are now available in large pack sizes for labeling up to 5 mg of antibody (in addition to the current pack size for 100 µg antibody). The SiteClick system allows simple and gentle site-selective attachment of detection molecules to heavy chain N-linked glycans (far from the antigen-binding domain) of primary antibodies, providing excellent reproducibility from labeling to labeling and antibody to antibody. Once the antibody's glycans are azido modified, a variety of detection molecules (Invitrogen™ SiteClick™ sDIBO alkynes)—including phycobiliproteins (e.g., R-PE), fluorescent dyes, Invitrogen™ Qdot™ probes, metal-chelating compounds, and other small molecules like biotin—are available for attachment to the antibody via click chemistry, allowing multiplex analysis with antibodies from the same species. Learn more at **thermofisher.com/ab-labeling**.

Product	Quantity	Cat. No.
SiteClick™ Antibody Azido Modification Kit	For 100 µg Ab labeling	S20026
	For 1 mg Ab labeling	S10900
	For 5 mg Ab labeling	S10901

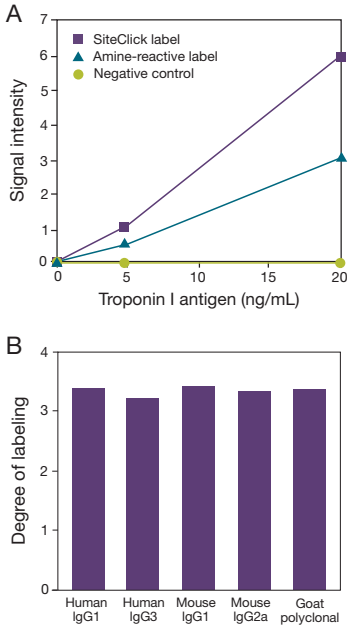

SiteClick antibody labeling. (A) Invitrogen™ SiteClick™ antibody labeling vs. amine-reactive labeling in a bead-based sandwich assay. **(B)** Demonstration of antibody-to-antibody consistency with SiteClick antibody labeling.

Invitrogen H3K4me3 antibody with demonstrated specificity in ChIP

Histone modifications serve as epigenetic signatures for gene expression. In partnership with EpiCypher Inc., we are using SNAP-ChIP™ (Sample Normalization and Antibody Profiling for Chromatin Immunoprecipitation) reagents to validate histone antibodies for specificity in ChIP applications. SNAP-ChIP™ Spike-In Controls are a panel of recombinant barcoded nucleosomes that are spiked into a ChIP workflow. qPCR amplification of the barcodes allows determination of the pull-down efficiency of the antibody and whether it recognizes any off-target modifications (demonstrated here with the Invitrogen™ H3K4me3 antibody). Learn more about our antibody validation at **thermofisher.com/antibodyvalidation** and search our antibody database at **thermofisher.com/antibodies**.

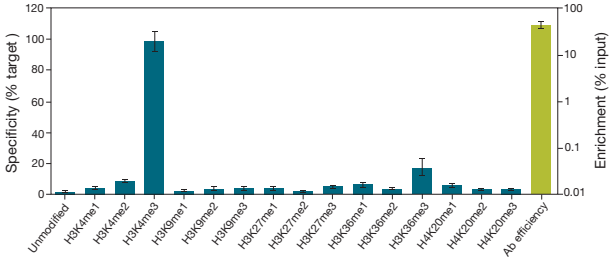

Histone modification specificity analysis. The EpiCypher™ SNAP-ChIP™ K-MetStat™ Panel was used to analyze the performance of Invitrogen™ H3K4me3 recombinant polyclonal antibody (Cat. No. 711958) in ChIP. Specificity (left y-axis) was determined by qPCR for each modified nucleosome in the SNAP-ChIP panel (x-axis). Green bar represents antibody efficiency and indicates percentage of the barcoded nucleosome target immunoprecipitated relative to input. All bars represent mean ± SEM.

New Hepatic Spheroid Kit with 3D-qualified hepatocytes

3D cell models have become important experimental tools for cancer biology and immunology, as well as for drug screening, discovery, and development. These models—including spheroids, tumor spheroids or tumoroids, and organoids—are relevant for many application areas because their microenvironment can mimic that of *in vivo* systems better than traditional 2D models. We now offer Gibco™ human spheroid-qualified hepatocytes to facilitate the production of 3D human liver models. When compared with traditional 2D hepatic cell cultures, hepatic spheroids generated using the Gibco™ Hepatic Spheroid Kit demonstrate:

- Increased cell-to-cell interactions
- Superior longevity (>21 days, 3x longer than most 2D hepatic cultures)
- Improved hepatocyte-specific function (e.g., higher levels of albumin, CYP, and MDR1 expression)

The Hepatic Spheroid Kit provides human spheroid-qualified hepatocytes, as well as media, supplements, and cultureware for 3D culture. Review our application data at **thermofisher.com/3dheps**.

Product	Quantity	Cat. No.
Hepatic Spheroid Kit	1 kit	A41390

New Pierce Dye and Biotin Removal Spin Columns and Filter Plates

Removing free dye from a protein sample after a labeling reaction is often difficult and time-consuming, but it is essential for accurate determination of dye-to-protein ratios. Thermo Scientific™ Pierce™ Dye and Biotin Removal Spin Columns and Filter Plates are highly specialized to produce exceptional protein recovery (for proteins >7 kDa), while quickly and effectively removing nonconjugated fluorescent dyes, biotinylation reagents, reducing agents, and crosslinkers. Product highlights include:

- High recovery—low-binding resin maximizes protein recovery
- Ease-of-use—no cumbersome column preparation or equilibration
- Fast—dye removal and protein recovery in less than 15 minutes

Product	Quantity	Cat. No.
Pierce™ Dye and Biotin Removal Spin Columns, 0.5 mL (Sample size per column: 50–120 µL)	5 columns 25 columns 2 x 25 columns	A44296S A44296 A44297
Pierce™ Dye and Biotin Removal Spin Columns, 2 mL (Sample size per column: 400–700 µL)	5 columns 25 columns	A44298 A44299
Pierce™ Dye and Biotin Removal Spin Columns, 5 mL (Sample size per column: 1–2 mL)	5 columns 25 columns	A44300 A44301
Pierce™ Dye and Biotin Removal Spin Columns, 10 mL (Sample size per column: 2–4 mL)	5 columns 5 x 5 columns	A44302 A44303
Pierce™ Dye and Biotin Removal Filter Plates, 96 well (Sample size per well: 40–100 µL)	2 plates 2 x 2 plates	A44304 A44305

Learn more at **thermofisher.com/small-molecule-removal**.

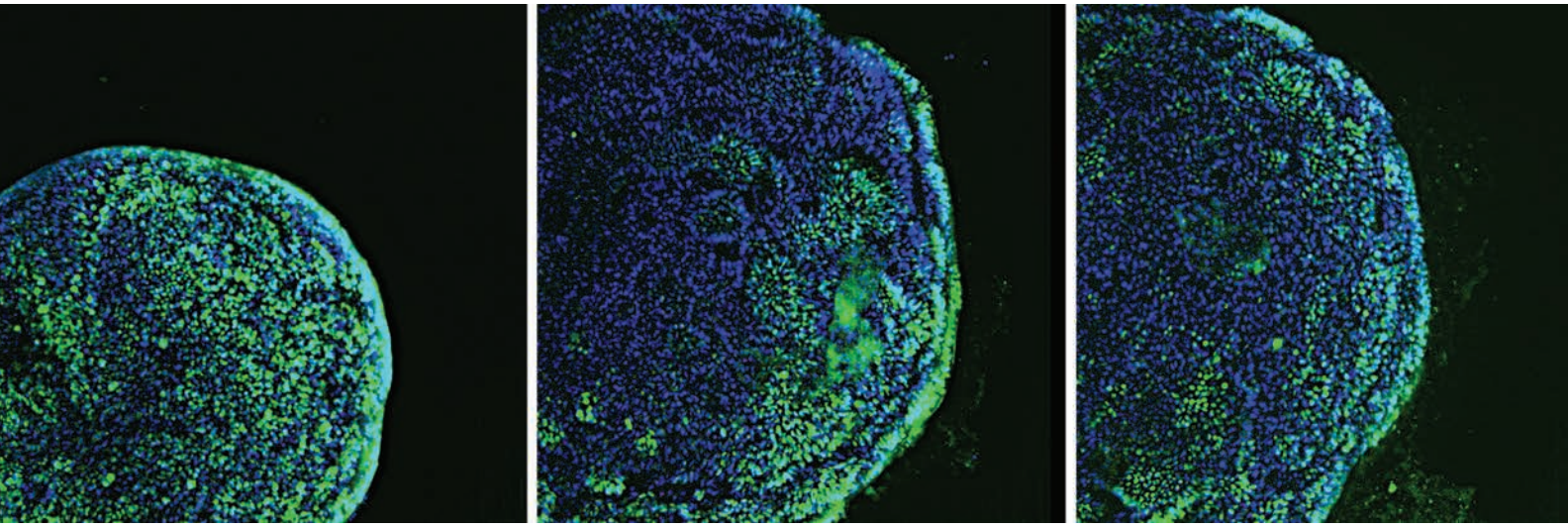

3D midbrain organoid model development

Floor plate differentiation of iPSC-derived dopaminergic neurons in 3D culture.

The drug development path—from hit discovery and lead advancement to the clinical space and commercialization—relies on accurate experimental data that are predictive of outcomes in downstream preclinical and clinical settings. Increasing the complexity of disease models with 3D organoids in the early stages of drug discovery is an approach that provides a more relevant cellular context, potentially more accurate physiological data in orthogonal experiments, and improved chances of eliminating false-positive hits during high-throughput screening. To realize these benefits, however, complex disease models must exhibit a similar cellular makeup and function as the organ under investigation. The development of 3D organoids that better represent the corresponding organ complexity enables researchers to better scale experiments, make data-driven decisions, and systemize those processes to speed discovery. →

Figure (above). ECM addition during floor plate specification supports prominent rosette-like structures in early organoids. See details in Figure 3 caption.

Highlighted here are some of the first steps in generating a functional 3D ventral midbrain neural organoid for modeling Parkinson's disease (PD). Achieving an organoid model of the brain—with the correct cell types that interact with each other and develop toward mature functionality—depends on many carefully defined parameters. These include physical factors such as those defined by basement membrane matrices, culture conditions, and spatial properties, as well as experimental factors such as how to best leverage the capabilities that advanced gene editing and imaging technologies provide. In the case of neurological diseases such as PD, research is hindered by a lack of access to diseased tissue. To model PD, we have developed a method for differentiating human induced pluripotent stem cells (iPSCs) to midbrain dopaminergic (DA) neurons, while also incorporating CRISPR technology to engineer iPSC-derived organoids such that they harbor either the PD-linked α-synuclein A30P mutation or its unaltered wild-type counterpart.

Comparison of 2D and 3D floor plate specification

Optimizing the conditions for organoid growth and structure is not a straightforward task, but with the right tools and technologies, *in vitro* disease models can be reproducibly generated at large scale. The Gibco™ PSC Dopaminergic Neuron Differentiation Kit enables the specification of iPSCs to midbrain floor plate cells. This kit is a set of three components (Floor Plate Specification Supplement, Floor Plate Cell Expansion Base and Supplement, and Dopaminergic Neuron Maturation Supplement) optimized for 2D midbrain floor plate specification, expansion, and maturation. In this discussion we demonstrate the use of this kit with and without an extracellular matrix (ECM) to specify floor plate cells and further differentiate DA neurons in 3D suspension culture. The schematic in Figure 1 describes the parallel floor plate derivation and DA maturation processes for 2D and 3D cultures.

The initial 3D workflow was kept as similar as possible to the optimized 2D schedule of passages and medium changes. In the 3D scenario, human iPSC spheroids in rotating suspension culture were dissociated and seeded into low-attachment 96-well, U-bottom (96U-well) microplates for floor plate specification in static suspension, then changed into expansion medium and maturation medium while in suspension without further passaging. As shown in Figure 1, the time requirements for specification and expansion in 3D were significantly reduced, with equivalent expression of floor plate markers. As expected, iPSCs that underwent 3D neural differentiation—based on their self-organization of progeny cells into organoids with brain-like structures and function—exhibited phenotypes not observed in 2D culture.

Organoid culture in the absence and presence of extracellular matrices

Attempts to improve the complexity of brain-like organoids are often accompanied by decreases in throughput and reproducibility, both of which impact research results and the scalability of disease models for drug discovery. As described in Figure 2, a comparison of four different 3D organoid culture methods was performed to assess early spheroid morphologies during differentiation (i.e., in rotating suspension versus U-well microplates; and without ECM, encapsulated in ECM, or suspended in ECM). To this end, cultures were grown in the absence of

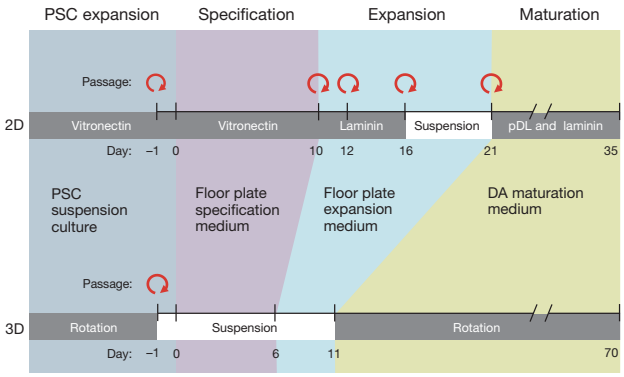

Figure 1. Comparison of 2D and 3D floor plate derivation processes using three different media prepared with the components provided in the PSC Dopaminergic Neuron Differentiation Kit. Starting with a human iPSC culture growing in Gibco™ Essential 8™ Medium (Cat. No. A1517001), we used the Gibco™ PSC Dopaminergic Neuron Differentiation Kit (Cat. No. A3147701) for the 2D and 3D floor plate derivation process. The top workflow shows 2D floor plate specification of an attached human iPSC culture, followed by multiple passages in expansion medium until day 21. Floor plate cells are then passaged onto poly-D-lysine (pDL) and laminin for differentiation of DA neurons up to day 35. The bottom workflow shows 3D midbrain organoid formation, beginning with human iPSCs in rotating suspension culture. These cells are dissociated and seeded into suspension culture for 3D floor plate specification. The floor plate specification medium is sequentially replaced with floor plate expansion medium and DA maturation medium while in suspension, without further passaging. As compared with 2D cultures, the duration of specification and expansion for 3D cultures can be shortened while maintaining equivalent expression of floor plate markers.

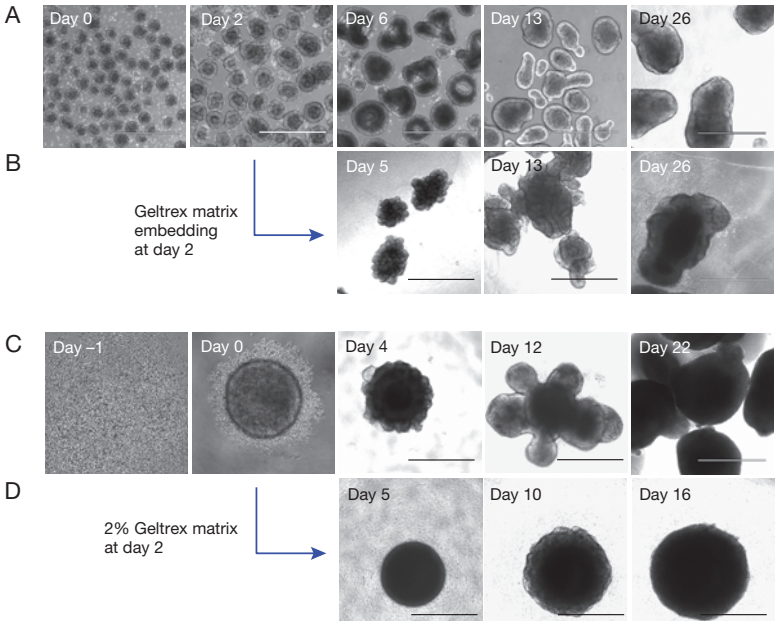

Comparison of methods shown in Figures 2A–D.

Method	Rotation (First 2 weeks)	ECM	Geltrex matrix
A	+	–	–
B	+	+	Encapsulate
C	–	–	–
D	–	+	Dilute

Figure 2. Organoid formation is boosted by ECM. The numbering of days corresponds to the 3D workflow shown in Figure 1. Floor plate specification and expansion of human iPSCs in rotating suspension **(A)** without ECM addition or **(B)** with ECM encapsulation at day 2 of floor plate specification in Gibco™ Geltrex™ LDEV-Free Reduced Growth Factor Basement Membrane Matrix (Cat. No. A1413201) diluted 1:1 in DMEM/F-12. **(C)** Floor plate specification and expansion of human iPSCs in static suspension culture in Thermo Scientific™ Nunclon™ Sphera™ 96U-Well Microplates (Cat. No. 174925) without ECM; organoids were transferred to rotating culture for maturation. **(D)** Floor plate specification and expansion of human iPSCs in static suspension culture in U-well microplates using floor plate specification medium supplemented with 2% Geltrex matrix at day 2; all other medium changes matched those in (C). Overall, we found that ECM encapsulation or a U-well microplate changes the morphology and complexity of midbrain floor plate organoids. Scale bar = 1,000 µm.

ECM and in the presence of 50% Gibco™ Geltrex™ LDEV-Free Reduced Growth Factor Basement Membrane Matrix (encapsulated in ECM) or a dilute ECM (suspended in 2% Geltrex matrix), and evaluated based on growth patterns, morphology, and maturation to understand the effects of different growth environments on the physical properties of the organoids.

Culture conditions that included ECM encapsulation or U-well microplates changed the morphology and complexity of midbrain floor plate organoids. Importantly, static suspension cultures grown in U-well microplates with addition of dilute ECM could reproduce some of the known benefits of ECM encapsulation, such as organoid complexity and faster neuronal maturation, without the difficulty and low throughput of encapsulation methods (method D, Figure 2). Surprisingly, U-well microplates increased the outgrowth of neural epithelia and yielded complex organoids, and the combination of U-well microplates and 2% Geltrex matrix produced a regular shape to the complex organoids (method D).

Confirmation of organoid morphology using high-content imaging and analysis

New instruments for imaging the whole brain, coupled with fluorescent gene reporters and reagents for optical clearing of tissue, can help shed light on neurodegenerative disease states [1]. The Thermo Scientific™ CellInsight™ CX7 LZR High-Content Analysis (HCA) Platform provides a powerful combination of fluorescence microscopy, image processing, automated cell measurements, and informatics tools to characterize the physical and biochemical properties of 3D organoids using a broad range of multiwell plate formats. When paired with onstage incubation, robotic plate handling, and the Thermo Scientific™ HCS Studio™ Cell Analysis Software, the CellInsight CX7 LZR platform can help to make 3D organoid research more scalable by taking advantage of rapid acquisition of z-stacks from multicellular structures.

To best understand the architectural effects that ECM has on floor plate specification in microwell-grown organoids, organoid culture →

methods C and D (Figure 2) were compared using HCA. Day 7 organoids grown without ECM or with dilute laminin or Geltrex matrix were cleared using the Invitrogen™ CytoVista™ 3D Cell Culture Clearing Reagent, immunostained for N-cadherin and counterstained with DAPI nuclear stain, and then imaged on the CellInsight CX7 LZR platform (Figure 3). N-cadherin (neural cadherin) is a transmembrane protein found to play a role in neural crest development, cell-to-cell adhesion, differentiation, and signaling [2]. N-cadherin antibody and DAPI staining showed that the addition of ECM increased the appearance of rosette-like structures on the surface of day 7 organoids.

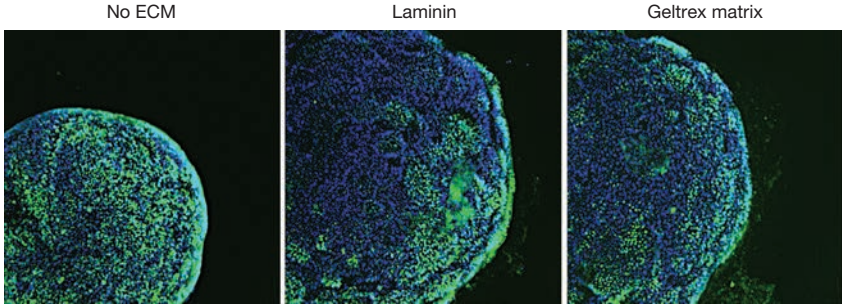

Figure 3. ECM addition during floor plate specification supports prominent rosette-like structures in early organoids. After specification by method C (Figure 2), static U-well microplate organoids (no ECM, left panel) were supplemented at day 2 with 200 µg/mL laminin (middle panel) or 2% Gibco™ Geltrex™ LDEV-Free Reduced Growth Factor Basement Membrane Matrix (Cat. No. A1413201) (right panel). Organoids were fixed on day 7 and labeled using Invitrogen™ N-cadherin monoclonal antibody (clone 3B9, Cat. No. 33-3900) in conjunction with Invitrogen™ Alexa Fluor™ 488 donkey anti–mouse IgG antibody (green, Cat. No. A21202) and DAPI (blue, Cat. No. D1306). Shown are maximal intensity projections of 8 µm optical sections, captured on the Thermo Scientific™ CellInsight™ CX7 LZR High-Content Analysis Platform (Cat. No. CX7A1110LZR).

Modeling Parkinson's disease with 3D organoid models

PD is characterized by the selective loss of DA neurons in the substantia nigra of the midbrain. This loss of DA neurons is observed in postmortem tissue along with Lewy bodies, which contain aggregates of phosphorylated α-synuclein protein. Lewy body formation in neurons has been described as the causative factor in DA neuron degeneration and the progressive loss of motor function associated with PD [3-5, also see *BioProbes 80* "Elucidate the underlying mechanisms of Parkinson's disease and other neurological disorders"]. Although only a minority of patients have a family history of PD, a growing number of genetic risk loci have been linked to sporadic cases and appear to influence susceptibility to environmental triggers.

In vitro models that reproduce the genetic basis of human disease can now be obtained by reprogramming patient cells to create iPSCs. Additionally, advances in gene editing technologies have led to the ability to create iPSC lines with any disease-relevant genome alteration. To apply these promising steps toward a reproducible 3D PD model, PD-associated single-nucleotide polymorphisms (SNPs) were engineered into iPSCs by CRISPR gene editing. Genes were edited in a stable Cas9-expressing iPSC line for high efficiency of cleavage and

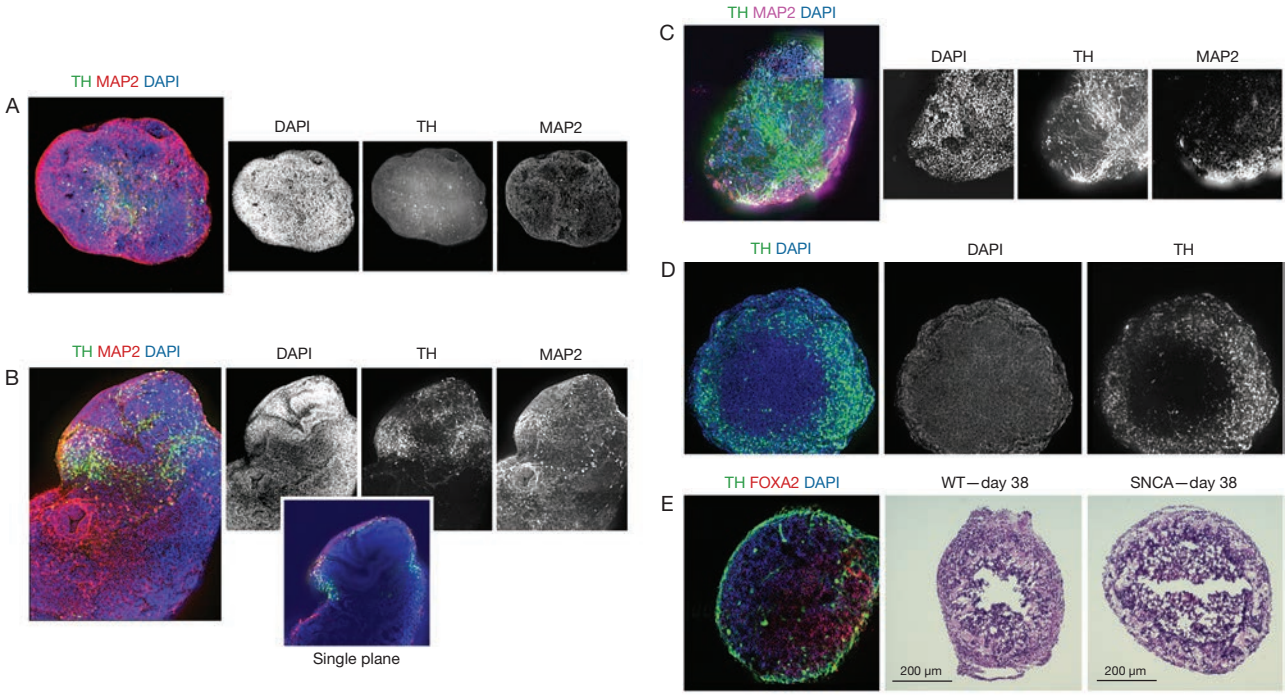

Figure 4. ECM encapsulation and U-well microplates increase organoid complexity and DA neuron yield. (A) Rotating suspension organoid (method A, Figure 2) at day 19 (early maturation): maximal intensity projection of Invitrogen™ MAP2 (Cat. No. PA5-17646) and tyrosine hydroxylase (TH) (Cat. No. MA1-24654) antibody staining and DAPI nuclear staining, as imaged on the Thermo Scientific™ CellInsight™ CX7 LZR High-Content Analysis Platform (Cat. No. CX7A1110LZR). **(B)** Encapsulated organoid (method B, Figure 2) at day 19: maximal intensity projection of MAP2 and TH antibody and DAPI staining. **(C)** Static U-well microplate organoid (method C, Figure 2) at day 19: maximal intensity projection of MAP2 and TH antibody and DAPI staining. **(D)** 23-day-old static U-well microplate organoid specified in the presence of 2% Gibco™ Geltrex™ LDEV-Free Reduced Growth Factor Basement Membrane Matrix (Cat. No. A1413201) at day 2 (method D, Figure 2): maximal intensity projection of TH antibody and DAPI staining. Midbrain organoids formed with ECM or in U-well microplates have a more complex epithelial morphology and earlier outgrowth of DA neurons. **(E)** 3-week-old static U-well microplate organoid specified in 2% Geltrex matrix: single optical section of TH and Invitrogen™ FOXA2 (Cat. No. 701698) antibody **(Cat. No. 701698)**and DAPI staining (left) and two images of hematoxylin/eosin–stained organoid sections (middle, right) from a SNCA wild-type (WT) or SNCA A30P mutant CRISPR iPSC line, which reveal thick bands of cells at the outside of the organoids surrounding a dense core of degrading cells. For immunodetection, primary antibodies were detected with Invitrogen™ Alexa Fluor™ 488 donkey anti–mouse IgG (Cat. No. A21202), Invitrogen™ Alexa Fluor™ 594 donkey anti–rabbit IgG (Cat. No. A21207), or Invitrogen™ Alexa Fluor™ 647 donkey anti–rabbit IgG (Cat. No. A32795) secondary antibody.

homology-driven repair. CRISPR editing was followed by one round of isolation by fluorescence-activated cell sorting (FACS), after which single cells showed robust clonal survival and growth when plated onto Gibco™ rhLaminin-521 in Gibco™ StemFlex™ Medium with Gibco™ RevitaCell™ Supplement. The precision of the mutations and clonality of the Cas9-expressing mutant and wild-type (WT) cell lines were verified by next-generation sequencing (NGS). One of the engineered SNPs creates the PD-linked A30P mutation in α-synuclein (SNCA). These SNCA mutant and WT control iPSC lines were differentiated toward midbrain organoids in U-well microplates with 2% Geltrex matrix in solution.

Early differentiation of the 3D cultures is marked by morphological change and expression of microtubule-associated protein 2 (MAP2) in neurons at the organoid surface. A portion of these are tyrosine hydroxylase (TH)-positive DA neurons (Figure 4). Comparison of organoid culture methods A, B, C, and D (Figure 2) demonstrates that midbrain organoids formed in free suspension without ECM (method A, Figure 4A) have a simple architecture with a single layer of neuronal cell bodies, whereas encapsulation in Geltrex matrix (method B, Figure 4B) increases neuroepithelial folding and the outgrowth of DA neurons. These effects are partially mimicked by organoid formation in low-attachment U-well microplates without (method C, Figure 4C) or with (method D, Figures 4D and 4E) a suspension of low-concentration Geltrex matrix.

Growth in this dilute ECM suspension (method D), however, outperforms encapsulation (method B) in promoting the maturation of midbrain organoids. The reddish-brown pigment neuromelanin is a byproduct of dopamine synthesis that gives dark coloration →

to the substantia nigra *in vivo* [6]. Midbrain organoids that have been encapsulated in ECM are dotted with pigment after many weeks of differentiation (Figure 5); organoids formed in U-well microplates with diffuse Geltrex matrix reach this milestone in about half the time, beginning to show neuromelanin pigmentation within 5 weeks.

Importantly, we generated midbrain organoids from WT and SNCA A30P iPSC lines using U-well microplates with dilute ECM and saw similarly complex epithelial morphology, earlier outgrowth of DA neurons, and evidence of rapid dopamine synthesis (Figures 4 and 5). Given the advantages in ease of use and faster maturation, we have chosen to continue midbrain organoid formation in U-well microplates with diffuse Geltrex matrix for our downstream functional and neurotoxicity studies.

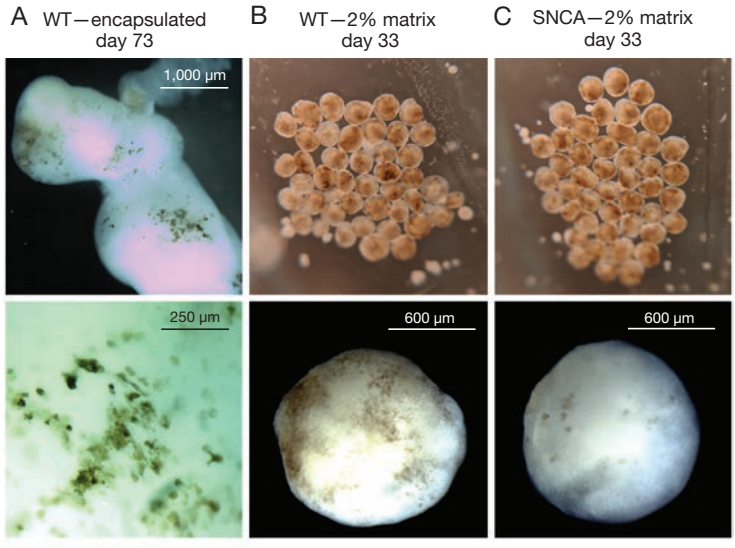

Figure 5. ECM promotes maturation of floor plate organoids. (A) Encapsulated organoid (method B, Figure 2) was imaged at day 73 without stains or dyes. The reddish-brown color suggests the presence of neuromelanin, a pigment that is a byproduct of dopamine synthesis [6]. **(B,C)** 23-day-old static U-well microplate organoid specified in the presence of 2% Gibco™ Geltrex™ LDEV-Free Reduced Growth Factor Basement Membrane Matrix (Cat. No. A1413201) at day 2 (method D, Figure 2) **(B)** from a SNCA wild-type (WT) CRISPR iPSC line or **(C)** from a SNCA A30P mutant CRISPR iPSC line. Earlier detection of neuromelanin in U-well microplate organoids with dilute Geltrex matrix suggests more rapid maturation of DA neurons.

Detecting action potentials in neural organoids using multielectrode arrays

Multielectrode arrays (MEAs) measure extracellular field potentials and are useful for studying neural circuit connectivity in monolayer cultures or organoids [7]. To detect spontaneous network activity in our midbrain model, we allowed single organoids to attach to an MEA with 16 electrodes, monitoring a surface area of 1.2 mm^2. Midbrain organoids generated by our method displayed spontaneous coordinated activity across the recording area in as little as 5 weeks of total differentiation time (Figure 6). *In vivo*, action potentials in the DA neurons of the substantia nigra are inhibited by excess dopamine [8]. Dopamine addition silenced the coordinated bursts we detected in midbrain organoids, confirming that these action potentials are driven by DA neurons.

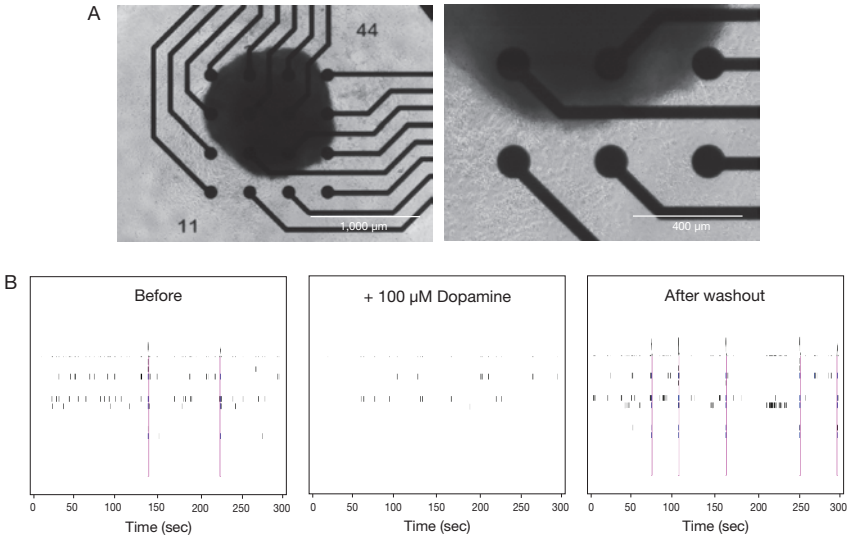

Figure 6. Floor plate organoids mature functionally. (A) Brightfield images show a static U-well microplate organoid specified in the presence of 2% Gibco™ Geltrex™ LDEV-Free Reduced Growth Factor Basement Membrane Matrix (Cat. No. A1413201) at day 2 (method D, Figure 2), cultured in suspension until day 21, and then allowed to attach in culture on a poly-D-lysine (pDL) and laminin–coated multielectrode array (MEA) for 14 days. **(B)** Raster plots of MEA recordings were derived from the plated U-well microplate organoid in (A). Each plot shows 300 sec of activity, first in maturation medium, second after addition of 100 µM dopamine, and third following washout of the dopamine. Vertical pink bars indicate detected network bursts. Midbrain organoids formed in U-well microplates with dilute Geltrex matrix can produce coordinated DA neuron activity in as little as 5 weeks.

In short, we have generated midbrain organoids from iPSCs by modifying the 2D protocol of the PSC Dopaminergic Neuron Differentiation Kit. This user-friendly method hastens functional maturation of DA neurons and makes promising steps toward a reproducible disease model for PD.

Advancing neuroscience research with 3D cell models

3D *in vitro* models of the brain and its disease states have become the focus of neuroscience research, due in part to the disappointing responsiveness of 2D culture models, but also to recent technological improvements that allow neuronal structures and functions to be observed in dense cell assemblies. Here we show our initial progress in generating organoids that show relatively rapid differentiation of DA neurons and capture several developmental events of the substantia nigra. We have engineered PD-relevant mutations into human iPSCs with CRISPR technology and are applying the derived midbrain organoids to model critical PD events. Ultimately, the use of iPSCs to build 3D brain models promises to advance our understanding of human disease mechanisms that are important to the development of therapeutic drugs and the implementation of cell and gene therapies. For more information on organoids, spheroids, and 3D cell culture, visit **thermofisher.com/3dculture**. ■

References

1. Zhu X, Xia Y, Wang X et al. (2017) *Neurosci Bull* 33:95–102. PMID 27535148
2. Derycke LD, Bracke ME (2004) *Int J Dev Biol* 48:463–476. PMID 15349821
3. Irvine GB, El-Agnaf OM, Shankar GM et al. (2008) *Mol Med* 14:451–464. PMID 18368143
4. Braak H, Del Tredici K (2016) *Cold Spring Harb Perspect Biol* 8:a023630. PMID 27580631
5. Moussaud S, Jones DR, Moussaud-Lamodière EL et al. (2014) *Mol Neurodegener* 9:43. PMID 25352339
6. Jo J, Xiao Y, Sun AX et al. (2016) *Cell Stem Cell* 19:248–257. PMID 27476966
7. Spira ME, Hai A (2013) *Nat Nanotechnol* 8:83–94. PMID 23380931
8. Lacey MG, Mercuri NB, North RA (1987) *J Physiol* 392:397–416. PMID 2451725

Product	Quantity	Cat. No.
Imaging instruments and reagents		
CellInsight™ CX7 LZR High Content Analysis Platform	1 each	CX7A1110LZR
CellInsight™ CX7 LZR High Content Analysis Platform and Store Standard Edition (SE) Software	1 each	CX7B1112LZR
CellInsight™ CX7 LZR High Content Analysis Platform with Store Standard Edition (SE) Software and Orbitor™ RS Plate Mover	1 each	CX7C1115LZR
CytoVista™ 3D Cell Culture Clearing Reagent	10 mL 30 mL 100 mL	V11326 V11315 V11316
HCS Studio™ 2.0 Cell Analysis Software	1 each	SX000041A
Onstage Incubator for CellInsight™ CX7 HCA Platform	1 each	NX7LIVE001
Culture reagents		
DAPI (4′,6-Diamidino-2-Phenylindole, Dihydrochloride)	10 mg	D1306
DMEM/F-12	500 mL 10 x 500 mL	11320033 11320082
Essential 8™ Medium	500 mL	A1517001
Geltrex™ LDEV-Free Reduced Growth Factor Basement Membrane Matrix	1 mL 5 mL	A1413201 A1413202
Laminin Mouse Protein, Natural	1 mg	23017015
Nunclon™ Sphera™ Microplates, 96U-Well Plate	1 case of 8	174925
Poly-D-Lysine	100 mL	A3890401
PSC Dopaminergic Neuron Differentiation Kit	1 kit	A3147701
rhLaminin-521	100 µg 1 mg	A29248 A29249
StemFlex™ Medium	500 mL	A3349401
RevitaCell™ Supplement (100X)	5 mL	A2644501
Antibodies		
FOXA2 Recombinant Rabbit Monoclonal Antibody (clone 9H5L7)	100 µg	701698
MAP2 Polyclonal Antibody	100 µL	PA5-17646
N-Cadherin Monoclonal Antibody (clone 3B9)	100 µg	33-3900
Tyrosine Hydroxylase (TH) Monoclonal Antibody (clone 185)	50 µL	MA1-24654

Characterizing functional immuno-oncology

Using flow cytometry and high-content imaging to evaluate innate immune function.

The field of immuno-oncology has expanded dramatically in the last few decades, producing novel immunotherapies designed to enhance or enable antitumor immune responses, overcome tumor evasion mechanisms, and promote conditions that favor immune protection. Immunotherapy may offer distinct advantages over conventional treatment modalities [1]. For example, tumor-specific immune cells have the ability to migrate to areas of the body that are inaccessible by surgery, to target microscopic disease and disseminated metastases, and to potentially act specifically against the tumor, thereby lowering the risk of damage to surrounding healthy tissue; nevertheless, severe toxicities may be associated with some particular immunotherapies.

In 2013, Chen and Mellman defined the series of immune system functions that specifically target and kill cancer cells as the cancer-immunity cycle [2], which involves the coordination of a myriad of checkpoint molecules and other cell-surface receptors, as well as soluble factors such as cytokines and chemokines. This complex series of anticancer immune responses is typically initiated by the release of tumor-derived antigens. The engulfment of these antigens by dendritic cells and their subsequent presentation to T cells drive the immune response. Once activated, effector T cells acquire the ability to destroy target cells by specifically recognizing tumor antigens displayed on the tumor cell surface (Figure 1). Trafficking of T cells to tumors, followed by infiltration of the T cells into tumors, leads to cancer cell death. Increasing levels of tumor antigens are then released, further driving the progression of the cycle.

Understanding the mechanisms of T cell–based immunity has led to many revolutionary cancer therapies, including (1) checkpoint blockade immunotherapies, which block either the immunosuppressive proteins on the surface of cancer cells or the T cell proteins that recognize them, thereby allowing T cells to mount an immune response, and (2) chimeric antigen receptor (CAR) T cell therapy, a form of adoptive cell therapy in which T cells are extracted from a patient, genetically engineered to express a CAR specific for a tumor antigen, cultured *ex vivo*, and then reintroduced back into the patient to attack tumor cells.

These therapeutic modalities, while clinically successful for many patients, are limited in their focus to T cells of the adaptive immune system. Recently, translational research has increasingly focused on the role of the innate immune system in antitumor immunity, as summarized by Demaria and colleagues in the cancer–innate immunity cycle [3]. These efforts have resulted in novel therapeutics such as CAR natural killer (NK) cells [4] and engineered antibodies designed to better recruit the cancer cell killers of the innate immune system: complement proteins, NK cells, and macrophages [5]. These approaches will hopefully benefit a larger percentage of patients and provide more scalable manufacturing, while reducing potential drug toxicity. Here we describe methods and assays to characterize the targeted killing of cancer cells by three different innate immune mechanisms: complement-dependent cell killing, NK cell–mediated cytotoxicity, and phagocytosis by macrophages (Figure 1).

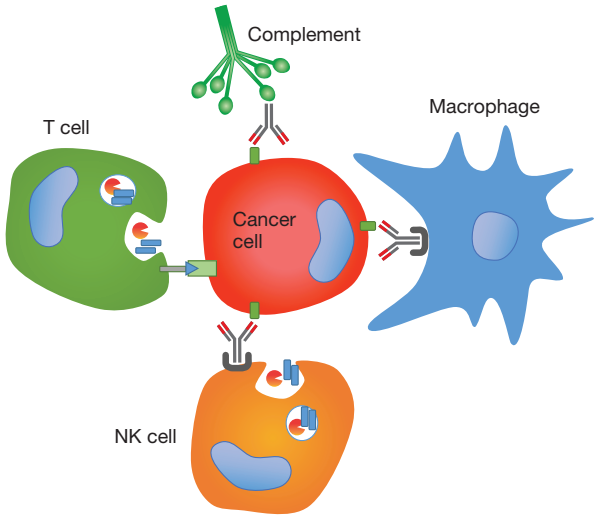

Figure 1. Mechanisms of cancer immunotherapy that employ both the adaptive and innate immune system. T cells form the backbone of the adaptive immune system, whereas the innate immune system is mediated by complement-dependent cytotoxicity (CDC), natural killer (NK) cell recruitment, and phagocytosis by macrophages.

Antibody-mediated complement-dependent cytotoxicity

When an antibody drug such as rituximab (an anti-CD20 monoclonal antibody) binds to the CD20 membrane protein on cancer cells in the presence of human serum, complement proteins in the serum initiate

a complement cascade, ultimately leading to CD20+ cell death while leaving CD20– cells unaffected. Although the mechanism of rituximab-mediated complement activation is not well understood, the structure of the rituximab–CD20 complex has recently been published and suggests a model for complement recruitment that involves rituximab crosslinking CD20 molecules into circular super-assemblies specifically designed to engage complement [6].

We used flow cytometry to evaluate complement-dependent cytotoxicity (CDC) induced by therapeutic antibodies. The specificity of complement-dependent killing for cells expressing CD20 can be demonstrated by first labeling CD20+ Ramos B and CD20– Jurkat cell lines with spectrally distinct Invitrogen™ CellTrace™ cell proliferation stains—we used CellTrace Violet and CellTrace Far Red dyes. The labeled cells were then combined in equal quantities, followed by the addition of fresh human serum, rituximab, and the cell viability dye Invitrogen™ SYTOX™ Green Dead Cell Stain, which is also spectrally distinct from the proliferation dyes used. After a 1-hour incubation at 37°C, cells were analyzed with the Invitrogen™ Attune™ NxT Flow Cytometer with Autosampler. This combination of three bright, spectrally distinct fluorescent dyes analyzed on the efficient (up to 10x faster than traditional cytometers), and flexible (up to 4 lasers and 16 detection channels) Attune NxT Flow Cytometer enables clear discrimination of targeted killing in a mixed population of cells. Figure 2 shows that CD20+ cells (labeled with CellTrace Violet dye) undergo significant cell death whereas CD20– cells (labeled with CellTrace Far Red dye) are unaffected.

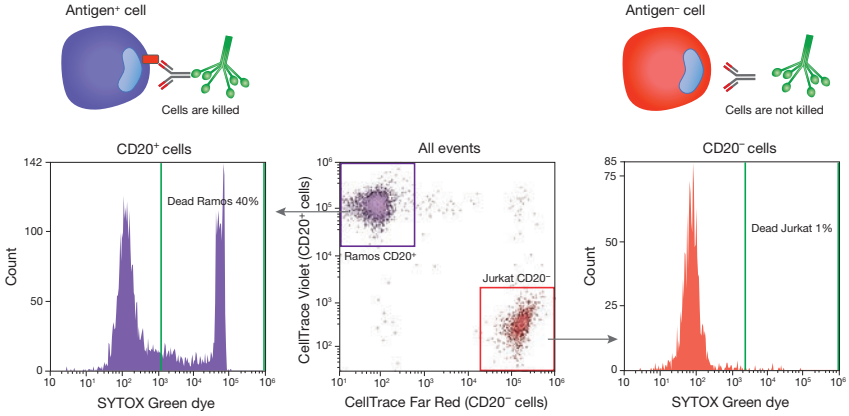

Figure 2. Specific complement-dependent cytotoxicity assay. Antibody binding to antigen-positive cells triggers the classical complement pathway, leading to cell death. CD20+ Ramos B cells were labeled with Invitrogen™ CellTrace™ Violet dye from the Invitrogen™ CellTrace™ Violet Cell Proliferation Kit (Cat. No. C34557). CD20– Jurkat cells were labeled with Invitrogen™ CellTrace™ Far Red dye from the Invitrogen™ CellTrace™ Far Red Cell Proliferation Kit (Cat. No. 34564). The two cell types were mixed 1:1 and incubated with 10 nM rituximab and 10% fresh human serum for 1 hr. Viability was measured with the Invitrogen™ SYTOX™ Green Dead Cell Stain (Cat. No. S34860). Cell analysis on the Invitrogen™ Attune™ NxT Flow Cytometer with Autosampler (Cat. No. A29004, Cat. No. 4473928) shows that cell death occurs only in antigen-positive (CD20+) cells.

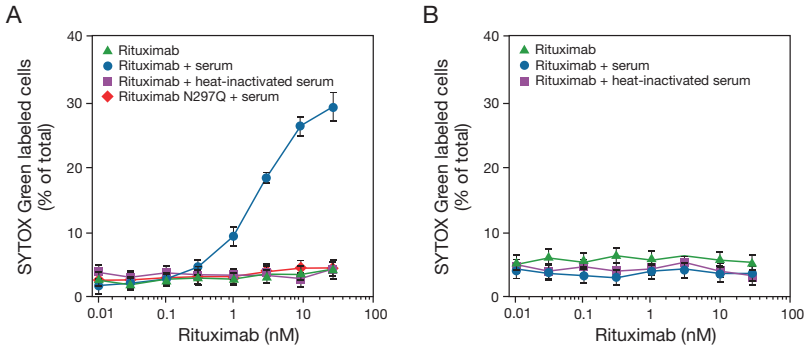

Figure 3. Flow cytometry screening for complement-dependent cytotoxicity. Using the cytotoxicity assay described in Figure 2 and either **(A)** CD20+ Ramos B cells or **(B)** CD20– Jurkat cells, we found that cell death only occurs with functional rituximab (not with mutated rituximab N297Q), active serum, and antigen-positive (CD20+) cells.

When characterizing the functional behavior of a therapeutic antibody, it is essential to test a range of antibody concentrations and conditions. This kind of screening experiment requires a robust flow cytometer and careful selection of reagents to provide clear results. Figure 3 shows the results of a typical antibody screening experiment using rituximab and CD20– and CD20+ cells, with analysis on the Attune NxT Flow Cytometer. We tested antibody concentrations across an 8-point dose-response curve, demonstrating the specificity of complement-dependent →

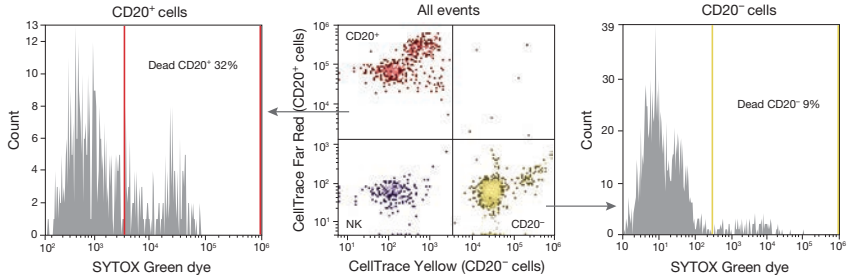

Figure 4. Specific antibody-dependent natural killer (NK) cell killing assay. NK cells were isolated from human peripheral blood mononuclear cells (PBMCs) using the Invitrogen™ Dynabeads™ Untouched™ NK Cells Kit (Cat. No. 11349D). NK cells were labeled with Invitrogen™ CellTrace™ Violet dye from the Invitrogen™ CellTrace™ Violet Cell Proliferation Kit (Cat. No. C34557); CD20+ Ramos B cells were labeled with Invitrogen™ CellTrace™ Far Red dye from the Invitrogen™ CellTrace™ Far Red Cell Proliferation Kit (Cat. No. 34564); and CD20– Jurkat cells were labeled with Invitrogen™ CellTrace™ Yellow dye from the Invitrogen™ CellTrace™ Yellow Cell Proliferation Kit (Cat. No. C34567). Cells were mixed 1:1:1 with 10 nM rituximab for 1 hr at 37°C, labeled with Invitrogen™ SYTOX™ Green Dead Cell Stain (Cat. No. S34860), and analyzed on the Invitrogen™ Attune™ NxT Flow Cytometer (Cat. No. A29004). The three cell types appear as distinct populations on a dot plot. NK cell antibody-dependent cell cytotoxicity (ADCC) is observed in CD20+ cells, while minimal death is observed in CD20– cells.

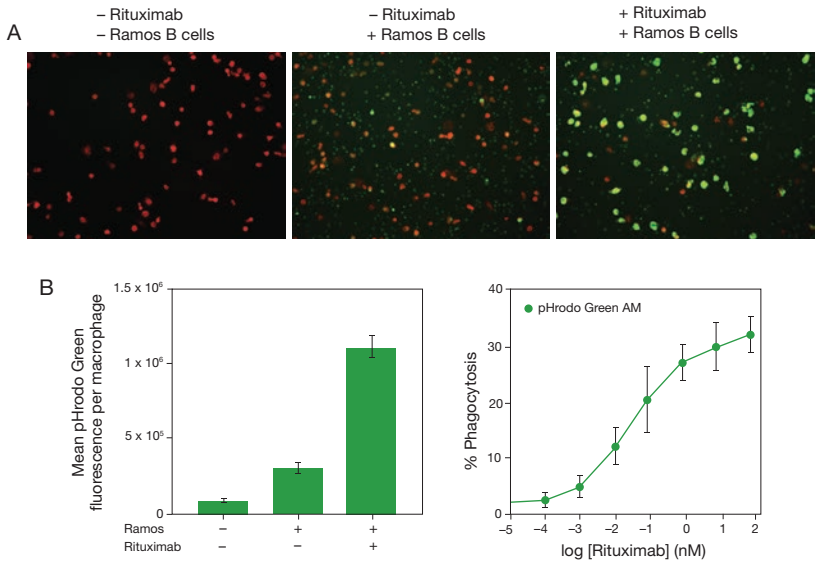

Figure 5. Quantitative imaging of antibody-dependent phagocytosis. Monocytes were isolated from human peripheral blood mononuclear cells (PBMCs) using Invitrogen™ Dynabeads™ Untouched™ Human Monocytes Kit (Cat. No. 11350D), then differentiated into macrophages for 7 days in Gibco™ RPMI 1640 Medium (Cat. No. 11875168) with 10% Gibco™ Fetal Bovine Serum (Cat. No. 26140087), 8% human serum, 1% Gibco™ GlutaMAX™ Supplement (Cat. No. 35050061), 20 mM HEPES, 1% Gibco™ Penicillin-Streptomycin (10,000 U/mL, Cat. No. 15140122), and 50 ng/mL Gibco™ M-CSF Recombinant Protein (Cat. No. PHC9501). Human monocyte–derived macrophages were cultured in a 96-well microplate before labeling with Invitrogen™ CellTrace™ Far Red dye (Cat. No. C34564). CD20+ Ramos B cells were labeled with Invitrogen™ pHrodo™ Green AM Intracellular pH Indicator (Cat. No. P35373) and added to the labeled macrophages with or without 10 nM rituximab and incubated for 4 hr at 37°C. Cells were **(A)** imaged and **(B)** analyzed with the Thermo Scientific™ CellInsight™ CX7 LZR High-Content Analysis Platform (Cat. No. CX7A1110LZR). Image-based analysis of pHrodo Green fluorescence in single cells provides a direct quantitative indication of antibody-mediated phagocytic events.

cell killing using one positive control (cells treated with rituximab and fresh human serum) and three negative controls (cells treated with rituximab only, rituximab and heat-inactivated serum, or mutated (nonfunctional) rituximab N297Q and serum). In CD20+ Ramos B cells, complement-dependent cytotoxicity only occurs with functional rituximab and active serum (Figure 3A). In contrast, CD20– Jurkat cells are completely unaffected by rituximab-mediated, complement-dependent cell killing (Figure 3B).

Antibody-mediated NK cell cytotoxicity

NK cells exhibit potent tumor-specific cytotoxicity based on a combination of activating and inhibitory receptors on their cell membrane surface. They can also kill target cells based on antibody-dependent cell cytotoxicity (ADCC), in which IgG antibodies (known as opsonizing antibodies) bind to tumor-associated antigens on cancer cells and to Fc receptors on NK cells, resulting in NK cell activation and cancer cell death.

The specificity and potency of ADCC can be demonstrated with an *in vitro* flow cytometry experiment. CD20+ Ramos B cells labeled with CellTrace Far Red dye and CD20– Jurkat cells labeled with CellTrace Yellow dye were combined with rituximab and labeled NK cells (previously isolated from peripheral blood and labeled with CellTrace Violet dye). After a 1-hour incubation, cells were labeled with SYTOX Green stain and analyzed using the Attune NxT Flow Cytometer (Figure 4). CD20+ cancer cells can be easily identified by the CellTrace Far Red tracking dye, and subsequently analyzed for SYTOX Green dye labeling to distinguish live and dead cell populations. The experimental controls demonstrate that

this cytotoxicity is entirely dependent on the presence of opsonizing antibody, as cell killing does not occur without sufficient rituximab (data not shown).

Antibody-dependent phagocytosis by macrophages

Antibody-opsonized cancer cells can also be recognized by Fc gamma receptors (FcγRs) on macrophages, leading to phagocytosis and killing of the cancer cells. This antibody-dependent cell phagocytosis (ADCP) is a major mechanism of action of therapeutic antibodies, which have been specifically developed to take advantage of the role macrophages play in the innate immune system. Accurate measurement of ADCP requires the use of fluorescent reagents that directly indicate the uptake of a cancer cell by a macrophage. Here we use the Thermo Scientific™ CellInsight™ CX7 LZR High-Content Analysis Platform to visualize and quantitatively analyze activation of the phagocytic pathway with the pH-sensitive Invitrogen™ pHrodo™ Green AM Intracellular pH Indicator. The pHrodo pH indicator, which is weakly fluorescent at neutral pH but increasingly fluorescent as the pH drops, can be used to quantify cytosolic pH in the range of 9–4, with a pKa of ~6.5 and excitation/emission of 509/533 nm.

CD20+ Ramos B cells were first labeled using the cell-permeant pHrodo Green AM ester and then added to macrophages labeled with CellTrace Far Red dye in the presence of varying concentrations of rituximab (Figure 5). With an adequate concentration of rituximab, the macrophages are observed to phagocytose the B lymphoma cells, which exhibit significantly more green fluorescence due to the acidification of the pH-sensitive pHrodo dye in the phagosome.

Instruments and reagents for immuno-oncology research

Thermo Fisher Scientific is developing new reagents and adapting existing reagents and instrumentation for the study of the immune system and its role within the cancer environment. To learn more about tools and technologies that enable immuno-oncology research, go to **thermofisher.com/immunooncology**, where you can download the Immuno-Oncology Product Resource Guide. Or, go to **thermofisher.com/flow-io** to download the Immuno-Oncology Flow Cytometry Guide, which reviews several central aspects of cancer research and provides detailed information about workflows for flow cytometry, biomarker profiling, and high-content cell imaging. ■

References

1. Dimberu PM, Leonhardt RM (2011) *Yale J Biol Med* 84:371–380. PMID 22180675
2. Chen DS, Mellman I (2013) *Immunity* 39:1–10. PMID 23890059
3. Demaria O, Cornen S, Daëron M et al. (2019) *Nature* 574:45–56. PMID 31578484
4. Liu E, Marin D, Banerjee P et al. (2020) *N Engl J Med* 382:545–553. PMID 32023374
5. Kamen L, Myneni S, Langsdorf C et al. (2019) *J Immunol Methods* 468:55–60. PMID 30880262
6. Rougé L, Chiang N, Steffek M et al. (2020) *Science* 367:1224–1230. PMID 32079680

Product	Quantity	Cat. No.
Instruments		
Attune™ NxT Flow Cytometer, blue/red/yellow/violet6	1 each	A29004
Attune™ NxT Flow Cytometer, blue/red/yellow/violet	1 each	A24858
Attune™ NxT Flow Cytometer Autosampler	1 each	4473928
CellInsight™ CX7 LZR High Content Analysis Platform	1 each	CX7A1110LZR
CellInsight™ CX7 LZR High Content Analysis Platform and Store Standard Edition (SE) Software	1 each	CX7B1112LZR
CellInsight™ CX7 LZR High Content Analysis Platform with Store Standard Edition (SE) Software and Orbitor™ RS Plate Mover	1 each	CX7C1115LZR
Culture and labeling reagents		
CellTrace™ Far Red Cell Proliferation Kit, for flow cytometry	20 assays 180 assays	C34572 C34564
CellTrace™ Violet Cell Proliferation Kit, for flow cytometry	20 assays 180 assays	C34571 C34557
CellTrace™ Yellow Cell Proliferation Kit, for flow cytometry	20 assays 180 assays	C34573 C34567
Dynabeads™ Untouched™ Human Monocytes Kit	1 kit	11350D
Dynabeads™ Untouched™ Human NK Cells Kit	1 kit	11349D
Fetal Bovine Serum	100 mL 500 mL 10 x 50 mL	26140087 26140079 A3160502
GlutaMAX™ Supplement	100 mL 20 x 100 mL	35050061 35050079
M-CSF Recombinant Human Protein	10 µg 100 µg	PHC9504 PHC9501
Penicillin-Streptomycin (10,000 U/mL)	20 mL 100 mL 20 x 100 mL	15140148 15140122 15140163
pHrodo™ Green AM Intracellular pH Indicator	50 µL	P35373
RPMI 1640 Medium	1 L 5 L 6 x 1 L	11875085 11875168 11875135
SYTOX™ Green Dead Cell Stain, for flow cytometry	1 mL	S34860

Immunodetection of proteins in the innate immune system

Antibodies for nucleic acid sensing pathways.

The innate immune system is an ancient germ line–encoded eukaryotic defense mechanism that usually forms the first-line host response to infection. In vertebrates, it includes physical barriers and general defense mechanisms, as well as the execution of an immediate and nonspecific immune response to incoming pathogens. The innate immune pathway comprises several families of pattern recognition receptors (PRRs) and adapter and signaling molecules that together result in the induction of a potent inflammatory response. This response in turn activates the adaptive and cell-mediated immune systems, which promote programmed cell death through phagocytosis, apoptosis, and necroptosis pathways.

PRRs, which include RIG-I–like receptors (RLRs), toll-like receptors (TLRs), and NOD–like receptors (NLRs), recognize various pathogen-associated molecular patterns (PAMPs) and danger-associated molecular patterns (DAMPs). PAMPs are biomolecules that are typically signs of an infection, such as extranuclear DNA and RNA (including specific viral nucleic acid motifs), bacterial cell wall and membrane components, and bacterial flagellin. In contrast, DAMPs are host biomolecules expressed by damaged, dying, or cancerous cells in the absence of infection, and their ability to stimulate the innate immune system leads to sterile inflammation [1]. DAMPs can play a significant role in activating aberrant (auto-immune) responses or protective immune responses in reaction to cardiovascular or neurodegenerative diseases, cancer, or nucleic acid immunization. Recently, agonists of pathways activated by PRRs have been under intense focus as potential targets for cancer immunotherapy because they can directly induce programmed cell death specifically in the tumor microenvironment; there are several in preclinical trials [2,3]. Here we describe several Invitrogen™ antibodies that are proving

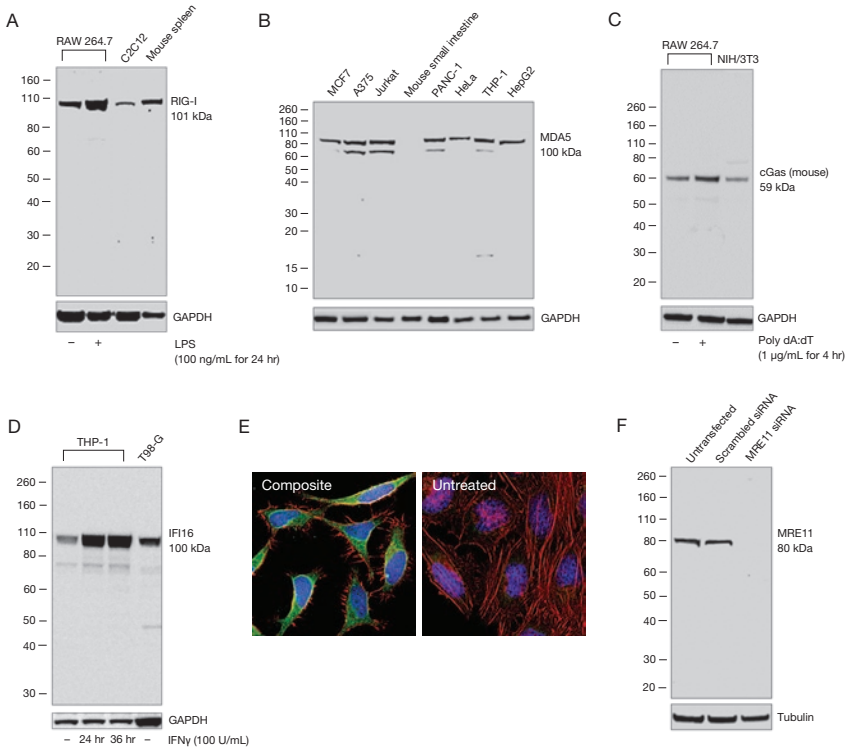

Figure 1. Assessment of the specificity of Invitrogen DNA and RNA sensor antibodies. (A) Western blot analysis of RIG-I antibody (clone 35H2L48, Cat. No. 700366) using whole-cell extracts from various cell lines and tissues. A 101 kDa band corresponding to RIG-I was observed in the cell lines and tissue tested, and this signal was enhanced in RAW 264.7 cells upon LPS treatment, which is known to increase RIG-I expression. **(B)** Western blot analysis of MDA5 antibody (clone 33H12L34, Cat. No. 700360) using whole-cell extracts from various cells and tissues. **(C)** Western blot analysis of cGAS (mouse) antibody (clone 10H1L5, Cat. No. 703149), showing increased expression of cGAS (mouse) in RAW 264.7 cells upon transfection with poly dA:dT (1 µg/mL for 4 hr). **(D)** Western blot analysis of IFI16 antibody (clone 8H37L1, Cat. No. 703147), showing increased expression of IFI16 in THP-1 cells treated with 100 U/mL IFNγ for 24 hr (lane 2) and for 36 hr (lane 3). **(E)** Immunofluorescence analysis of IFI16 using IFI16 polyclonal antibody (green, Cat. No. PA5-76462), showing increased expression of IFI16 in HeLa cells upon IFNγ treatment. **(F)** Western blot analysis of MRE11 polyclonal antibody (Cat. No. PA3-16527) using whole-cell extracts from A431 cells transfected with MRE11 siRNA. For the western blot analyses, primary antibodies were probed with Invitrogen™ Goat Anti–Rabbit IgG Superclonal™ Recombinant Secondary Antibody, HRP (Cat. No. A27036), detected using the Thermo Scientific™ Pierce™ ECL Western Blotting Substrate (Cat. No. 32106), and imaged using the Invitrogen™ iBright™ FL1000 Imaging System.

useful for the study of the nucleic acid sensing pathways, highlighting the strategies we employ to ensure target specificity for each antibody.

Antibody detection of nucleic acid sensors

Nucleic acid sensors, an important class of PRRs, are characterized according to whether they recognize RNA or DNA. The RIG-I–like receptors (RLRs), for example, are a family of cytosolic, structurally related RNA helicases that include RIG-I, MDA5, and LGP2. These receptors recognize "nonself" RNA structures in the cytoplasm, such as double-stranded RNA (dsRNA) and 5´-triphosphate RNA (5´-3pRNA), as well as aberrantly localized RNA that can result, for example, from ionizing radiation or chemotherapy. Such RNA-based PAMPs are commonly associated with viral infection, and mice lacking either RIG-I or MDA5 show increased susceptibility to viruses [4]. Furthermore, injection of 5´-3p–containing siRNAs into mice tumor models has been shown to induce RIG-I–dependent pathways and the recruitment of NK or $CD8^+$ T cells to the tumor site, leading to the production of IFNγ, tumor regression, and a prolonged life span [5,6]. Similarly, injection of the synthetic ligand poly I:C into epithelial ovarian cancer cells has been shown to activate MDA5, trigger tumor apoptosis, induce inflammatory cytokines, and enhance expression of HLA class 1 molecules [7]. Figures 1A and 1B show validation* data for Invitrogen™ rabbit recombinant antibodies that recognize RIG-I and MDA5; target specificity for the RIG-I antibody has been verified by cell treatment with lipopolysaccharide (LPS), which is known to increase RIG-I expression.

Like RNA sensors, DNA sensors also produce an inflammatory response that can lead to programmed cell death and may be harnessed to improve patient outcomes after ionizing radiation or chemotherapy [8]. DNA sensors specifically detect the presence of cytoplasmic DNA, which is indicative of infection or cell damage; nuclear and mitochondrial DNA do not activate these pathways. The DNA sensor cGAS recognizes dsDNA and synthesizes the second messenger cyclic GMP-AMP (2´3´-cGAMP) upon ligand binding. Injection of cyclic dinucleotides into mice tumor models results in cGAS activation, improved tumor clearance, and enhanced survival [3]. The DNA sensor IFI16 recognizes single-stranded DNA (ssDNA) from human cytomegalovirus and HSV-1 in the cytoplasm of human macrophages and is essential for induction of type I interferon response in these infections. MRE11 is a DNA damage sensor that recognizes dsDNA in the cytoplasm and activates downstream signaling [8]. Figures 1C–1F show validation data for antibodies that recognize the cGAS, IFI16, and MRE11 DNA sensors; target specificity for each antibody was verified using cell treatments known to increase expression of target proteins (cGAS and IFI16 antibodies) or siRNA to silence expression (MRE11 antibody).

Antibody detection of adapter and signaling molecules

The nucleic acid sensor proteins associate with various adapter proteins, which in turn signal downstream components. For example, RLRs activate a protein called MAVS (mitochondrial antiviral signaling protein), which is localized in mitochondria and peroxisomes, leading to its oligomerization and filament formation [9]. MAVS knockout →

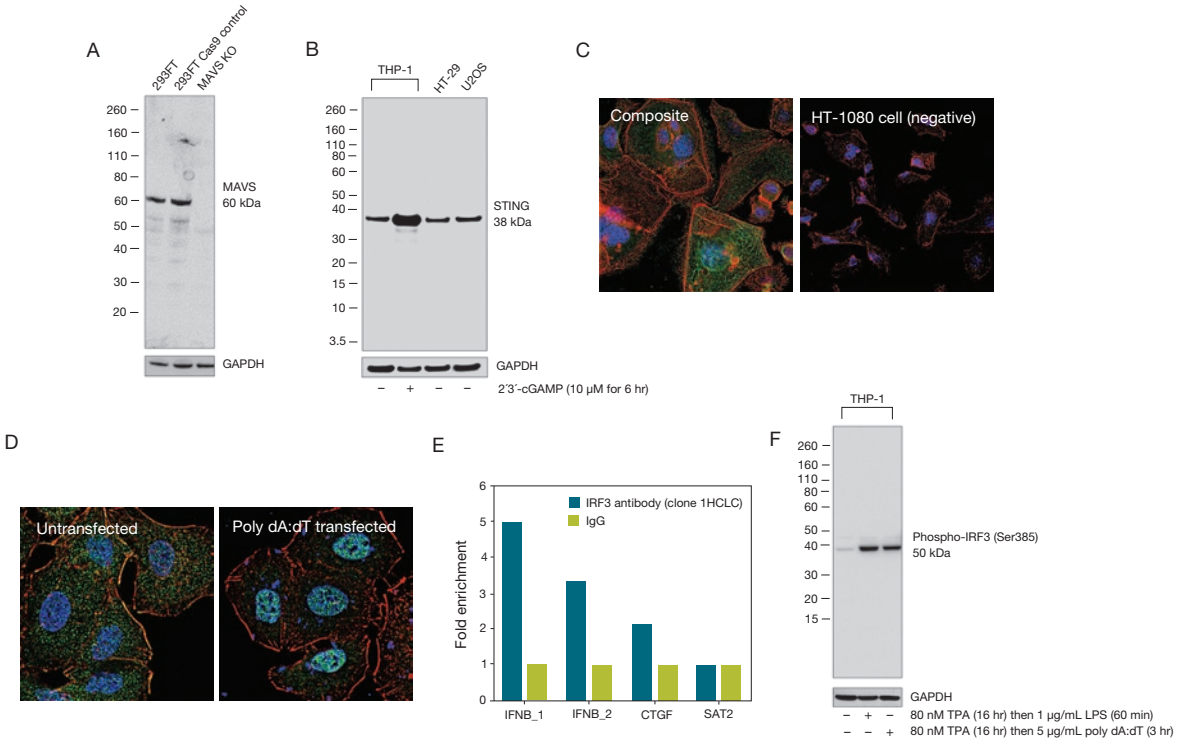

Figure 2. Assessment of the specificity of Invitrogen adapter and signaling protein antibodies. (A) Western blot analysis of MAVS antibody (clone 20H41L5, Cat. No. 703153) using cell membrane–enriched extracts from a CRISPR-Cas9 mediated knockout (KO) of MAVS in 293FT cells. **(B)** Western blot analysis of STING antibody (clone 2H1L5, Cat. No. 702993), showing increased STING expression in THP-1 cells upon treatment with 2′3′-cGAMP. **(C)** Immunofluorescence analysis of MyD88 polyclonal antibody (Cat. No. PA5-19919), showing increased MyD88 expression in SK-BR-3 cells as compared with HT-1080 cells. **(D)** Immunofluorescence analysis of IRF3 antibody (green; clone 3H32L10, Cat. No. 703682), showing IRF3 expression in the nucleus of A549 cells transfected with poly dA:dT and in the cytoplasm in untransfected control cells. **(E)** Chromatin immunoprecipitation (ChIP) analysis of IRF3 (clone 1HCLC, Cat. No. 712217) using PCR primer pairs for two different promoter regions in the IFNB gene, for the CTGF promoter (positive control), and for SAT2 satellite repeats (negative control). ChIP analysis demonstrated IRF3 antibody specificity through the detection of IRF3 enrichment at specific gene loci. **(F)** Western blot analysis of phospho-IRF3 (pSer385) polyclonal antibody (Cat. No. PA5-36775), showing an increase in phospho-IRF3 (pSer385) upon treatment of THP-1 cells with TPA and LPS, and with TPA and poly dA:dT. For the western blot analyses, primary antibodies were probed with Invitrogen™ Goat Anti–Rabbit IgG Superclonal™ Recombinant Secondary Antibody, HRP (Cat. No. A27036), detected using the Thermo Scientific™ Pierce™ ECL Western Blotting Substrate (Cat. No. 32106), and imaged using the Invitrogen™ iBright™ FL1000 Imaging System.

mice can no longer induce interferon and other inflammatory cytokines in response to viral infections. The DNA sensors cGAS and IFI16 both engage the endoplasmic reticulum–localized protein STING (stimulator of interferon genes). MyD88 (myeloid differentiation marker 88) is an adapter that plays an important role downstream of endosomal DNA sensor TLR9 [8]. Figures 2A–2C show the validation data for MAVS, STING, and MyD88 antibodies; antibody specificities have been verified using a CRISPR knockout model (MAVS antibody), cell treatment with 2′3′-cGAMP (STING antibody), and relative expression (MyD88 antibody).

Activated MAVS, STING, and MyD88 lead to the phosphorylation and activation of the protein kinase TBK1. Phosphorylated TBK1 further phosphorylates and activates the transcription factor IRF3. IRF3 usually resides in the cytoplasm; however upon TBK1 phosphorylation, it dimerizes and translocates from the cytoplasm to the nucleus. In the nucleus, it binds to the promoters of genes containing the ISRE (interferon-stimulated response element) sequence and activates the transcription of IFNβ and a subset of interferon-stimulated genes. Phosphorylated TBK1 also activates the transcription factor NFkB, leading to its nuclear translocation and transcriptional activation of

proinflammatory cytokines [8,9]. Figures 2D–2F show the validation data from three IRF3 antibodies, two that recognize total IRF3 and one that recognizes phospho-IRF3 (pSer385). Target specificity for the two Invitrogen™ IRF3 rabbit recombinant polyclonal antibodies is shown by observing the poly dA:dT–mediated translocation of IRF3 from the cytoplasm to the nucleus using immunofluorescence (Figure 2D) and by detecting pull down of IFN promoter sequences but not those from the SAT2 locus using chromatin immunoprecipitation (ChIP) (Figure 2E). The Invitrogen™ polyclonal antibody for phospho-IRF3 (pSer385) was used to detect phosphorylated IRF3 on western blots in extracts from cells treated with TPA followed by either LPS or poly dA:dT (Figure 2F).

Antibody tools for investigating the immune system

Nucleic acid sensing pathways are increasingly being investigated for their therapeutic potential in treating infection, cancer, and degenerative diseases. Table 1 lists Invitrogen™ antibodies that recognize several components of these pathways. Search for these and other target-verified, application-tested antibodies at **thermofisher.com/antibodies**. To learn more about our validation methodology, visit **thermofisher.com/antibodyvalidation**. ■

*The use or any variation of the word "validation" refers only to research use antibodies that were subject to functional testing to confirm that the antibody can be used with the research techniques indicated. It does not ensure that the product(s) was validated for clinical or diagnostic uses.

References

1. Chen GY, Nuñez G (2010) *Nat Rev Immunol* 10:826–837. PMID 21088683
2. Iurescia S, Fioretti D, Rinaldi M (2018) *Front Immunol* 9:711. PMID 29686682
3. Li K, Qu S, Chen X et al. (2017) *Int J Mol Sci* 18:404. PMID 28216575
4. Kato H, Takeuchi O, Sato S et al. (2006) *Nature* 441:101–105. PMID 16625202
5. Poeck H, Besch R, Maihoefer C et al. (2008) *Nat Med* 14:1256–1263. PMID 18978796
6. Ellermeier J, Wei J, Duewell P et al. (2013) *Cancer Res* 73:1709–1720. PMID 23338611
7. Kübler K, tho Pesch C, Gehrke N et al (2011) *Eur J Immunol* 41:3028–3039. PMID 21728171
8. Paludan SR, Bowie AG (2013) *Immunity* 38:870–880. PMID 23706668
9. Loo YM, Gale M Jr (2011) *Immunity* 34:680–692. PMID 21616437

Table 1. Invitrogen™ antibodies for nucleic acid sensing pathways.

Target protein	Rabbit monoclonal, recombinant monoclonal, or recombinant polyclonal Ab (Cat. No.)	Rabbit polyclonal Ab (Cat. No.)	Mouse monoclonal Ab (Cat. No.)
DNA and RNA sensors			
RIG-I	700366		
MDA5	700360		
cGAS (mouse)	703149	PA5-56820	
IFI16	703147	PA5-39180, PA5-51690, PA5-76462	
MRE11		PA3-16527, PA5-31262	
DHX9		PA5-19542, PA5-55754	
Adapter proteins			
STING	702993		
MAVS	703153		14-9835-82
MyD88		PA5-19919	
Signaling proteins			
IRF3	703682, 712217	PA5-20087, PA5-78026	14-9947-82
Phospho-IRF3 (pS385)		PA5-36775	
NFkB p50	710450	51-3500	MA5-15860, MA5-15870
NFkB p65	710048	PA1-186, PA5-16545, 51-0500	33-9900
Phospho-NFkB p65 (pS536)	MA5-15160		
NFkB p52		PA5-27340	

*Go to **thermofisher.com/antibodies** for detailed information about each of these antibodies, including advanced verification data. To learn more about our two-part antibody validation methods—target specificity verification and functional application validation—visit **thermofisher.com/antibodyvalidation**.

Phenotyping on the front lines

Flow cytometry antibodies for identifying tissue-resident memory T cells.

Identified about a decade ago, tissue-resident memory T cells (T_{RM}) provide antigen-specific protection from pathogens and viruses in peripheral tissues. Characterized by their residency in tissues and distinct inability to recirculate, T_{RM} have been identified in lung, skin, liver, brain, intestinal, and mucosal tissues [1-4]. While initial studies focused on their persistence at sites of previous infection and their long-lived role in combating reinfection (through immediate effector function and accelerated recruitment of circulating immune cells), T_{RM} have also been reported to accumulate in the tumor microenvironment, including those of epithelial (ovarian, pancreatic, colorectal, and lung) and nonepithelial (malignant glioma and melanoma) origin [5].

The efficacy of immune checkpoint inhibitors (anti–PD-1, anti–PD-L1, and others) in cancer treatment has led researchers to postulate that T_{RM} are key players in the tumor microenvironment, capable of initiating and maintaining antitumor responses due to their high levels of expression of inhibitory receptors. Potential mechanisms of action include rapid and local antigen-specific proliferative responses, with expression of effector molecules to promote inflammation and immune cell recruitment and differentiation (IFNγ, TNFα, IL-2, IL-17) and to direct target-cell lysis (perforin, granzyme B) [6,7]. Therefore, increased activation of T_{RM} is thought to be a fruitful strategy for enhancing current immunotherapy approaches and vaccination efficacy. In this article, we will review common T_{RM} markers and address the development of T_{RM} flow cytometry panels. Thermo Fisher Scientific offers a wide variety of Invitrogen™ primary antibodies and antibody conjugates for flow cytometry that recognize positive and negative markers for T_{RM} (Table 1).

Key cell-surface markers for T_{RM}

The peripheral blood T cell population contains a variety of subsets that can be identified by expression of CD45RA, CCR7 (CD197), and CD62L (L-selectin). These subsets include naïve ($CD45RA^+ CCR7^+ CD62L^+$), central memory (T_{CM}; $CD45RA^- CCR7^+ CD62L^+$), and effector memory (T_{EM}; $CD45RA^- CCR7^- CD62L^-$) T cells, as well as terminally differentiated effector memory cells re-expressing CD45RA (T_{EMRA}; $CD45RA^+ CCR7^- CD62L^-$) [8]. T_{EM} play an important role in immune surveillance and are a major subset of both $CD4^+$ and $CD8^+$ T cell populations found in peripheral tissues [7,9]. In contrast, T_{CM} survey secondary lymphoid organs for cognate antigen, while naïve cells are typically localized to the blood, spleen, and lymph nodes [8].

CD69: Human T_{RM} are typically associated with the expression of the surface markers CD69, CD49a (integrin α1), and CD103 (integrin αE); these markers, along with CD44, are useful for studying mouse T_{RM}. Although CD69 is a marker of early T cell activation, most T_{RM} express CD69 under steady-state conditions, without expression of other activation markers such as CD25, CD38, and HLA-DR [10]. CD69 is therefore an important distinguishing cell-surface marker constitutively expressed on T_{RM} in most tissues, and it functions as a critical antagonist of S1PR1 (CD363) activity [11]. The $CD69^+$ T_{RM} population is phenotypically and transcriptionally distinct from recirculating $CD69^-$ memory T cells in both tissues and blood, each having a defined gene expression signature that includes molecules associated with adhesion, migration, and regulation [6,7].

CD49a: CD49a (integrin α1) is also an important marker expressed in some T_{RM}, as it acts with CD29 (integrin β1) to form the heterodimeric molecule VLA-1, which can bind collagen and laminin and promotes tissue residency [5,12].

CD103: CD103 (integrin αE) expression in T_{RM} is variable [7]. CD103 is upregulated after exposure to TGF-β, and it complexes with integrin β7 on the T cell surface to allow adherence through binding to CD324 (E-cadherin) on epithelial cells [11]. CD103 expression is restricted to $CD8^+$ T_{RM} in mucosal sites and skin [7,8,9]. T_{RM} that exist outside of epithelial tissues generally lack CD103 expression, although they may express other adhesion molecules such as LFA-1, which is a heterodimeric integrin composed of CD11a (LFA-1α) and CD18 (LFA-1β). In mice, LFA-1 is present on $CD103^-$ liver-resident T_{RM} and is thought to allow binding of CD54 (ICAM-1) on liver sinusoidal endothelial cells. It is not yet known if this marker is expressed on human liver-resident T_{RM} [13].

CD44: CD44 is a C-lectin–containing glycoprotein that is expressed on leukocytes and other cell types and serves as a receptor for hyaluronic acid (HUA), which is an extracellular matrix component produced by vascular endothelial cells and other immune cells [11]. CD44 also binds to other matrix proteins like fibronectin, laminin, and collagen [11]. In mice, CD44 is considered a core marker with a functional role

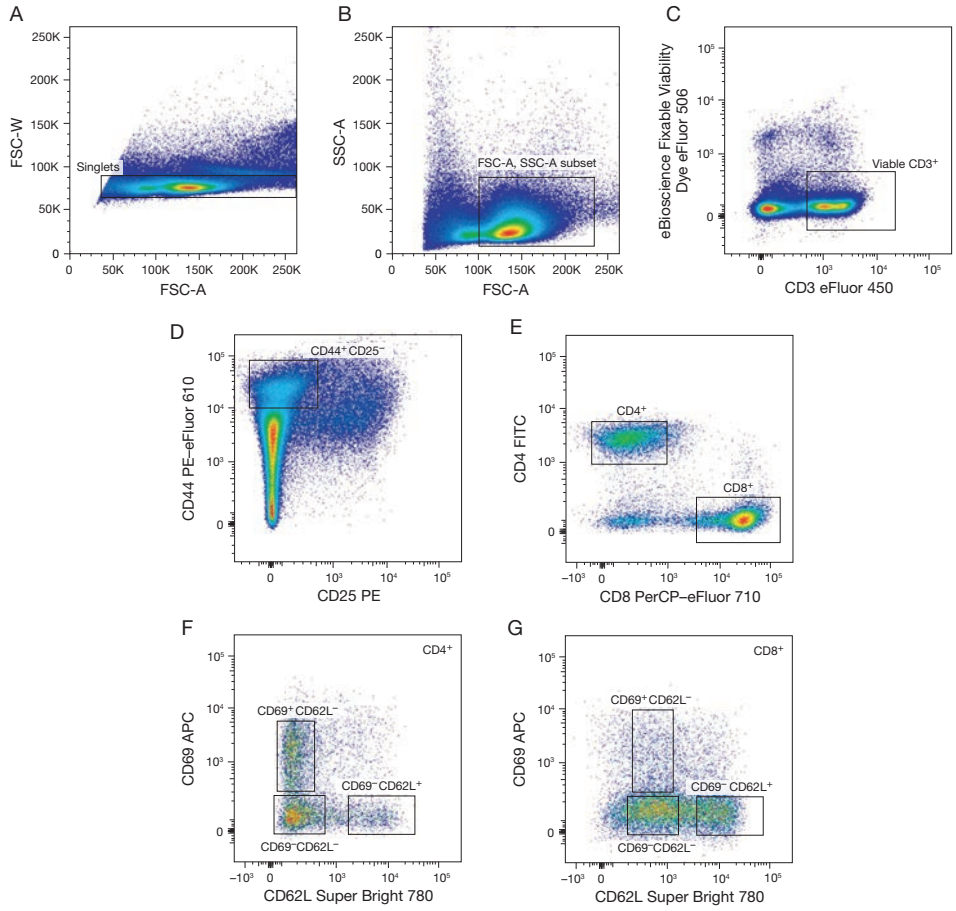

Figure 1. Example of a flow cytometry panel for T_{RM}. C57BL/6 mouse lymph node cells were stained with Invitrogen™ eBioscience™ CD3 eFluor™ 450, CD44 PE–eFluor™ 610, CD25 PE, CD62L Super Bright 780, CD4 FITC, CD8 PerCP–eFluor™ 710, and CD69 APC monoclonal antibodies. Viability was determined using Invitrogen™ eBioscience™ Fixable Viability Dye eFluor™ 506 (Cat. No. 65-0866-18). For analysis, viable CD3+ T cells **(C)** were gated from singlet-gated **(A)** mouse lymph node cells **(B)**. These CD3+ T cells were further gated by CD44+ and CD25− expression (memory and activation/Treg phenotype markers, respectively) **(D)**, and then into CD4+ and CD8+ subsets **(E)**. CD69 and CD62L expression identifies T_{RM} cells (CD69+CD62L−), T_{CM} cells (CD69−CD62L+), and T_{EM} cells (CD69−CD62L−) in the CD4+ population **(F)** and the CD8+ population **(G)**. **For Research Use Only. Not for use in diagnostic procedures. Not for resale.** Super Bright Polymer Dyes are sold under license from Becton, Dickinson and Company.

in T_{RM} biology. Its expression, however, does not distinguish the T_{RM} subset from other CD8+ T cell populations, and it is mainly used as a marker of previous T cell activation, as it also labels T_{CM} and T_{EM} [11]. The role of CD44 in T_{RM} may include regulation of cell–cell interactions, cell adhesion, migration, or lymphocyte activation.

T_{RM} surface marker signature

The Farber lab at the Columbia University Medical Center has reported a core T_{RM} surface marker signature consistent across tissues and diverse human donors and expressed in both CD4+ and CD8+ T cells [7]. In their approach, T_{RM} are identified as CD69+, while T_{EM} are CD69−. When compared to CD69− T_{EM}, CD69+ T_{RM} show upregulated expression of CD103 (integrin αE), CD49a (integrin α1), CRTAM (CD355), CD186 (CXCR6), CD279 (PD-1), MKP3 (DUSP6), and IL-10. Notably, expression of CD186 (CXCR6) allows for migration into peripheral tissues. Furthermore, CD69+ T_{RM} show downregulated expression of S1PR1, CD62L, CX3CR1, and KLF2 relative to CD69− T_{EM}, a phenotype consistent with the retention of T_{RM} within tissues [7,9].

Other markers of interest expressed specifically in CD8+ CD69+ T_{RM} are ICOS and IRF4 [7]. CD101 is also upregulated on CD8+ T_{RM}, as compared with CD4+ T_{RM} in the lung and spleen, and may be involved in inhibition of T cell activation and proliferation [7,9]. CD28 and CD127 (IL-7R) may be useful for delineating cell activation and homeostasis [4]. T_{RM} development and maintenance are regulated by CD122 (IL-15R) and CD127 (IL-7R), and the latter receptor is expressed on a majority of CD69+ T_{RM} [6]. Other homing and retention markers may →

be utilized to distinguish T_{RM} in specific compartments, such as CLA (CD162, PSGL-1), CCR8, CCR10, FABP4, and FABP5 on skin-resident T_{RM}, and CCR9 and integrin α4β7 (LPAM-1) on intestine-resident T_{RM} [5].

The study of transcriptional regulation in T_{RM} is ongoing. Perhaps as a function of their diversified tissue distribution with myriad metabolic niches, T_{RM} are currently thought to rely on combinations of transcription factors, and a unifying lineage-restricted master regulator has not yet been identified [11]. That said, several transcription factors have been identified as important for T_{RM} tissue residency. T_{RM} are reported to downregulate the T-box transcription factors EOMES (negative) and T-bet (low) following TGF-β signaling [5,6,14]. RUNX3 enhances granzyme B and CD103 expression, whereas NOTCH1 appears to regulate metabolism in T_{RM} [6]. Other transcription factors may contribute to tissue residency programs, such as BLIMP-1 and HOBIT, which can repress CCR7, S1PR1, KLF2, and TCF-1 expression (although some reports suggest the role of HOBIT in T_{RM} may be limited) [5,9]. Current research is focused on identifying the components of the general and tissue-specific signaling pathways that regulate T_{RM}.

Flow cytometry panels for T_{RM}

Taking these data into consideration, flow cytometry panels for T_{RM} may include a core set of markers such as CD45, CD69, CD3, CD4, CD8, CD279 (PD-1), CD103 (integrin αE), CD186 (CXCR6), CD19 (negative), CD45RA (negative), CCR7 (negative), and CD62L (negative) (Figure 1). Further clarity would be provided by inclusion of CX3CR1 and S1PR1 markers in the panels [6]. CD44 is useful in mouse T_{RM} panels [9]. T_{RM} may also upregulate CD28 and CD127 (IL-7R), although this upregulation appears to depend on tissue localization [7,8]. Further memory phenotypes may be identified using KLRG1 and CD27. Tissue-specific homing markers, such as LFA-1, CCR8, CCR10, CLA, FABP4, FABP5, CCR9, and integrin α4β7 (LPAM-1) may also be of interest [6].

Antibody selection tools for your flow cytometry panels

T_{RM} are an important and still-emerging subset in oncology, potentially other disease research, and vaccine design. Further studies are needed to illuminate their development and roles in disease protection and progression. Table 1 lists selected Invitrogen™ flow cytometry antibodies and antibody conjugates for the study of T_{RM}. Search our complete portfolio of primary and secondary antibodies for flow cytometry, immunofluorescence, western blotting, ELISAs, and other applications at **thermofisher.com/antibodies**. ■

References

1. Mami-Chouaib F, Tartour E (2019) *Front Immunol* 10:1018. PMID 31191515
2. Mueller SN, Mackay LK (2016) *Nat Rev Immunol* 16:79–89. PMID 26688350
3. Schenkel JM, Fraser KA, Masopust D (2014) *J Immunol* 192:2961–2964. PMID 24600038
4. Thome JJ, Yudanin N, Ohmura Y et al. (2014) *Cell* 159:814–828. PMID 25417158
5. Corgnac S, Boutet M, Kfoury M et al. (2018) *Front Immunol* 9:1904. PMID 30158938
6. Behr FM, Chuwonpad A, Stark R et al. (2018) *Front Immunol* 9:1770. PMID 30131803
7. Kumar BV, Ma W, Miron M et al. (2017) *Cell Rep* 20:2921–2934. PMID 28930685
8. Thome JJ, Farber DL (2015) *Trends Immunol* 36:428–435. PMID 26072286
9. Steinbach K, Vincenti I, Merkler D (2018) *Front Immunol* 9:2827. PMID 30555489
10. Sathaliyawala T, Kubota M, Yudanin N et al. (2013) *Immunity* 38:187–197. PMID 23260195
11. Topham DJ, Reilly EC (2018) *Front Immunol* 9:515. PMID 29632527
12. Ray SJ, Franki SN, Pierce RH et al. (2004) *Immunity* 20:167–179. PMID 14975239
13. McNamara HA, Cai Y, Wagle MV et al. (2017) *Sci Immunol* 2:eaaj1996. PMID 28707003
14. Mackay LK, Wynne-Jones E, Freestone D et al. (2015) *Immunity* 43:1101–1111. PMID 26682984

Table 1. Invitrogen™ flow cytometry antibodies and selected antibody conjugates for the study of tissue-resident memory T cells.

Species	Marker type	Marker	Location	Notes	Clone (selected* Cat. No.)
Mouse	Core marker	CD69	Surface	Found on most T_{RM}; also expressed by activated cells	H1.2F3 (12-0691-82)
	General phenotype (not tissue-specific)	CD45	Surface	General lymphocyte marker	30-F11 (12-0451-82)
		CD3	Surface	General T cell marker	145-2C11 (12-0031-82); 17A2 (12-0032-82); eBio500A2 (12-0033-82)
		CD4	Surface	$CD4^+$ T cell subset marker	GK1.5 (12-0041-82); RM4-5 (12-0042-82); RM4-4 (12-0043-82)
		CD8	Surface	$CD8^+$ T cell subset marker	53-6.7 (12-0081-82)
		CD279 (PD-1)	Surface	Highly expressed on T_{RM}	J43 (12-9985-82); RMP1-30 (12-9981-82)
		CD101	Surface	Subsets of T_{RM}	Moushi101 (12-1011-82)
		CD11a	Surface	Subunit of LFA-1	M17/4 (12-0111-82)
		CD44	Surface	Expression gradient: naïve < effector < memory T cells	IM7 (12-0441-82)
		CD127 (IL-7R)	Surface	Subsets of T_{RM}	A7R34 (12-1271-82)
		KLRG1	Surface	Negative or low expression on T_{RM}	2F1 (12-5893-82)
		CCR7 (CD197)	Surface	Negative on T_{RM}; expressed by T_{CM}	4B12 (12-1971-82)
		CD62L (L-selectin)	Surface	Negative on T_{RM}; expressed by T_{CM}	MEL-14 (12-0621-82)
		CD45.1 CD45.2	Surface	May be used for parabiosis studies	A20 (12-0453-82) 104 (12-0454-82)
		Blimp-1	Nuclear		5E7 (12-9850-82)
	Mucosal and barrier sites	CD103 (integrin αE)	Surface	Subsets of T_{RM}	2E7 (12-1031-82)
	Skin and liver	CD186 (CXCR6)	Surface	Subsets of T_{RM}	DANID2 (12-9186-82)
	Skin	CD183 (CXCR3)	Surface		CXCR3-173 (12-1831-82)
	Liver	LFA-1	Surface		M17/4 (12-0111-82); M18/2 (12-0181-82)
Human	Core marker	CD69	Surface	Found on most T_{RM}; also expressed by activated cells	FN50 (12-0699-42)
	General phenotype (not tissue-specific)	CD45	Surface	General lymphocyte marker	HI30 (12-0459-42); 2D1 (12-9459-42)
		CD3	Surface	General T cell marker	UCHT1 (12-0038-42); SK7 (12-0036-42); OKT3 (12-0037-42); HIT3a (12-0039-42)
		CD4	Surface	$CD4^+$ T cell subset marker	RPA-T4 (12-0049-42); OKT4 (12-0048-42); SK3 (12-0047-42)
		CD8	Surface	$CD8^+$ T cell subset marker	RPA-T8 (12-0088-80); OKT8 (12-0086-42); HIT8a (12-0089-42); SK1 (12-0087-42)
		CD45RA	Surface	Naïve T cell marker; negative on T_{RM}	HI100 (12-0458-42)
		CD45RO	Surface	Memory T cell marker	UCHL1 (12-0457-42)
		CD279 (PD-1)	Surface	Highly expressed on T_{RM}	MIH4 (12-9969-42); eBioJ105 (14-2799-80)
		CD127 (IL-7R)	Surface	Subsets of T_{RM}	eBioRDR5 (12-1278-42)
		NOTCH1	Intracellular	Possible T_{RM} metabolic marker	mN1A (12-5785-82)
		CRTAM (CD355)	Surface	Upregulated on some T_{RM} subsets (adhesion molecule)	Cr24.1 (12-3559-42)
		S1PR1 (CD363)	Surface	Downregulated on T_{RM}	SW4GYPP (50-3639-42)
		CX3CR1	Surface	Downregulated on T_{RM} vs. circulating T_{RM}	2A9-1 (12-6099-42)
		CCR7 (CD197)	Surface	Negative on T_{RM}; expressed by T_{CM}	3D12 (12-1979-42)
		CD62L (L-selectin)	Surface	Negative on T_{RM}; expressed by T_{CM}	Dreg-56 (12-0629-42)
		CD101	Surface	Subsets of T_{RM}	BB27 (14-1019-82)
	Mucosal and barrier sites	CD103 (integrin αE)	Surface	Subsets of T_{RM}	B-Ly7 (12-1038-42)
	Lung and skin	CD49a (integrin α1)	Surface		TS2/7 (46-9490-42)
	Lung	CD183 (CXCR3)	Surface		CEW33D (12-1839-42)
	Skin	CD194 (CCR4) CLA	Surface		D8SEE (12-1949-42) HECA-452 (50-9857-82)
	Lymph node	CD184 (CXCR4) CD185 (CXCR5)	Surface		12G5 (12-9999-42) MU5UBEE (12-9185-42)
	Liver	LFA-1	Surface		HI111 (11-0119-42); 6.7 (12-0189-42); R3.3 (BMS103FI)

*Antibodies are available as several different conjugates and in multiple packagings. Go to **thermofisher.com/antibodies** to see a complete listing.

Assess cell health and function in 2D and 3D cell cultures

Optimizing microplate assay protocols for spheroid cultures.

3D cell models are now increasingly being adopted for cancer, immuno-oncology, neuroscience, and other research areas because their microenvironments more closely resemble the micro-anatomy of *in vivo* systems (organized tissues, organs, and tumors), which contain a complex and dynamic set of cell types, chemical gradients, and extracellular matrix (ECM) components. The complexity of 3D cell structures can present a challenge when using cell health assays and protocols originally developed for monolayer (2D) cell cultures. Here we highlight a few basic considerations for adapting and optimizing our microplate-based 2D cell culture viability assays for spheroid cultures, focusing on the optimization of reagent concentration and incubation time.

Determine the optimal reagent concentration

The optimal reagent concentration for spheroid cultures will provide a high assay-specific signal with the lowest possible nonspecific background, resulting in a high signal-to-noise (S/N) ratio. An assay with a high S/N ratio shows greater sensitivity for detecting changes in cell health due to cell treatments, such as exposure to drugs or test compounds. To demonstrate this effect, we assayed spheroids derived from human lung epithelial cells (A549 cells) using the Invitrogen™ CyQUANT™ XTT Cell Viability Assay, a colorimetric microplate assay originally developed to assess 2D cell viability as a function of redox potential (Figure 1). We compared the recommended reagent concentration (1X) with a 2X concentration, in the absence or presence of increasing concentrations of the cytotoxic drug gambogic acid, and found that doubling the reagent concentration increased the S/N ratio, and thus the assay sensitivity. We recommend testing a wide range of reagent concentrations to find the most appropriate one for your 3D assay.

Determine the optimal reagent incubation time

The optimal reagent incubation time for spheroid cultures can be determined by running a time-course experiment and plotting assay signal as a function of incubation time. Figure 2 shows an example of such a time-course experiment using an established microplate viability assay that determines redox potential by measuring the reduction of resazurin to the highly fluorescent (and intensely colored) resorufin. Using the Invitrogen™ PrestoBlue™ HS Cell Viability Reagent with various incubation times, we compared the fluorescence generated by A549 cells in a 2D monolayer with that of A549 cell–derived spheroids. The assay protocol recommends incubation times for 2D cell culture of 10 minutes to 3 hours, within the linear range of the time-course curve. Based on our experiments with spheroids, we recommend extending the incubation time—to between 5 and 10 hours—to maximize signal and stay within the linear range of this curve.

Learn more about microplate assays for 3D cultures

Thermo Fisher Scientific offers a wide range of microplate assays for the detection of cell viability, health, and function that can be easily optimized for 3D cell culture systems. Find out more about our microplate assays and microplate readers at **thermofisher.com/microplateassays**, and explore our 3D cell culture products at **thermofisher.com/spheroid**. ■

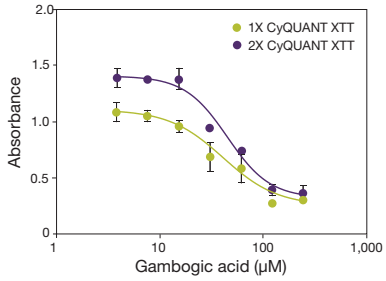

Figure 1. Determine the optimal reagent concentration. Human lung epithelial cells (A549 cells) were plated in Thermo Scientific™ Nunclon™ Sphera™ 96U-Well Microplates (Cat. No. 174925) at 5,000 cells/well in complete MEM for 19 hr to allow spheroid formation. The surface of these plates exhibits extremely low ECM binding properties, which inhibits cell attachment and promotes spheroid formation. The A549 cell spheroids were then treated with 7 concentrations of gambogic acid for 26 hr and assayed for cell health with the Invitrogen™ CyQUANT™ XTT Cell Viability Assay (Cat. No. X12223) using the recommended (1X) or 2X reagent concentration. All measurements were made using the Thermo Scientific™ Varioskan™ LUX Multimode Microplate Reader (Cat. No. VLBLATD0).

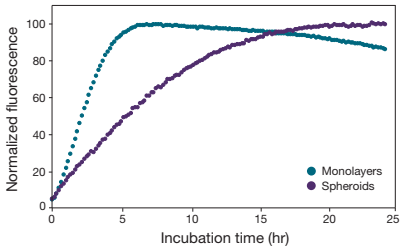

Figure 2. Determine the optimal reagent incubation time. A549 cell spheroids (prepared as described in Figure 1) and A549 cell monolayers were assayed at various incubation times with Invitrogen™ PrestoBlue™ HS Cell Viability Reagent (Cat. No. P50200). All measurements were made using the Thermo Scientific™ Varioskan™ LUX Multimode Microplate Reader (Cat. No. VLBLATD0).

Product	Quantity	Cat. No.
CyQUANT™ XTT Cell Viability Assay	1 kit	X12223
PrestoBlue™ HS Cell Viability Reagent	25 mL 100 mL	P50200 P50201
Varioskan™ LUX Multimode Microplate Reader	1 each	VLBLATD0

Introducing the new Qubit Flex Fluorometer: DNA, RNA, and protein quantitation with flexible throughput

Accurate and precise quantitation of up to 8 samples simultaneously.

DNA, RNA, and proteins are typically quantified using fluorescence or UV absorbance. Previous studies have shown that measurements using selective fluorescent stains are far more accurate and sensitive than those that rely on UV absorbance, which detects any molecule that absorbs at 260 nm, including DNA, RNA, protein, free nucleotides, and excess salts. Moreover, UV spectrophotometry is often not sensitive enough to accurately measure low concentrations of DNA and RNA. The Invitrogen™ Qubit™ platform combines benchtop fluorometers with Invitrogen™ Qubit™ assays to provide an optimized, easy-to-use, dedicated system for the accurate and reliable fluorescence-based quantitation of nucleic acid and protein.

Current fluorometers read one sample at a time, which works well for low-throughput needs. When processing multiple samples, however, this low-throughput workflow will significantly increase the time required to obtain results. Additionally, sequential processing of samples can contribute to a decrease in the accuracy and precision of the quantitation results. A benchtop fluorometer that can read a group of samples simultaneously provides significant time savings and reduced variability.

To address this need, we have developed the Invitrogen™ Qubit™ Flex Fluorometer, the newest member of the Qubit™ family of fluorescence-based quantitation instruments. Similar to the Invitrogen™ Qubit™ 4 Fluorometer, the Qubit Flex Fluorometer is a benchtop device with an intuitive interface and large 8-inch, state-of-the-art color touchscreen, designed explicitly for the highly accurate quantitation of DNA, RNA, and protein. The Qubit Flex Fluorometer increases quantitation throughput with the ability to measure up to 8 samples at once (Figure 1). The time it takes to generate quantitation measurements using the Qubit Flex Fluorometer is significantly less than that required with single-sample readers, due in part to a 50% reduction in hands-on time. In addition to time savings, the Qubit Flex Fluorometer's ability to read 8 samples simultaneously helps to reduce assay variability and yield reproducible data because each sample is exposed to identical quantitation conditions. The Qubit Flex Fluorometer is compatible with the same optimized Qubit assay reagents as the Qubit 4 Fluorometer, each of which has been formulated to cover a broad range of target molecule concentrations and provide sensitive quantitation with as little as 1 µL of sample.

Figure 1. Flex your throughput—introducing the Qubit Flex Fluorometer. The Invitrogen™ Qubit™ Flex Fluorometer (Cat. No. Q33327) provides the same great performance you expect from the Invitrogen™ Qubit™ Fluorometers but now has built-in flexibility to quantify DNA, RNA, or protein in 1 to 8 samples simultaneously.

Speedy quantitation

To measure the time needed to quantify an increased number of samples, we used the Invitrogen™ Qubit™ 1X dsDNA HS Assay Kit (Cat. No. Q33231) with the Qubit Flex Fluorometer, the Qubit 4 Fluorometer, and a single-sample fluorometer from another supplier. The time required to prepare and quantify 1, 8, 24, 48, and 96 samples of 4 different concentrations of lambda DNA (0.1, 1, 5, and 10 ng/µL) on the each of the three fluorometers was recorded. This study demonstrates that time savings are realized with the Qubit Flex Fluorometer using batches of as few as 8 samples, and efficiency multiplies as the number of samples increases (Figure 2). When compared with a single-sample fluorometer, the Qubit Flex Fluorometer provides a reduction of up to 50% in total time-to-data (from preparation to measurement of the samples) for higher numbers of samples. In addition, the Qubit Flex Fluorometer can save data for up to 10,000 samples, and you can transfer data to the Connect cloud-based platform using Wi-Fi, a USB drive, or ethernet cable. →

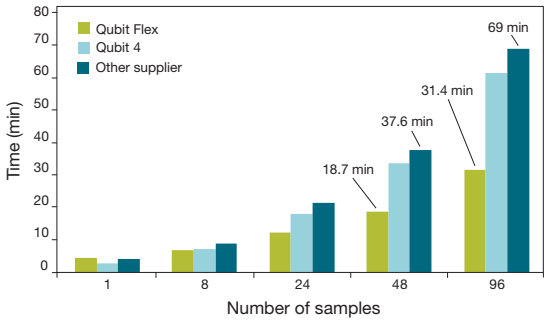

Figure 2. The Qubit Flex Fluorometer reduces time-to-data by up to 50%. A time study comparing the Invitrogen™ Qubit™ Flex Fluorometer with both the Invitrogen™ Qubit™ 4 Fluorometer and another supplier's single-sample fluorometer showed time-to-data reduced by up to 50% using the Invitrogen™ Qubit™ 1X dsDNA HS Assay Kit (Cat. No. Q33230) with up to 96 samples.

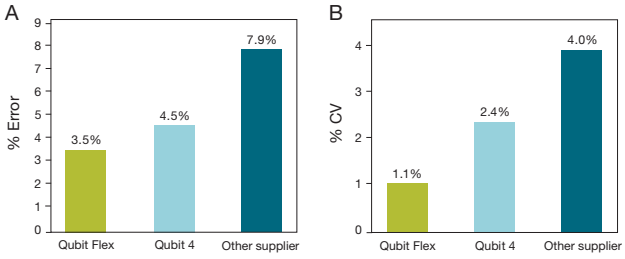

Figure 3. Qubit platforms deliver better accuracy and precision than other manufacturers. Invitrogen™ Qubit™ 1X dsDNA HS and Qubit™ dsDNA BR Assay Kits (Cat. No. Q33230, Q32850) were run with 4 DNA sample concentrations (BR assay: 2, 20, 50, and 100 ng/µL; HS assay: 0.1, 1, 5, and 10 ng/µL) in 8 replicates on the Invitrogen™ Qubit™ Flex Fluorometer, Invitrogen™ Qubit™ 4 Fluorometer, and another supplier's single-sample fluorometer. **(A)** The percent relative error (lower is more accurate) and **(B)** percent CV (lower is more precise) were measured for each data point and averaged across all concentrations for each instrument.

Accurate, precise measurements

To determine the accuracy and precision of quantitation measurements, we used the Invitrogen™ Qubit™ 1X dsDNA HS and Qubit™ dsDNA BR Assay Kits with the Qubit Flex Fluorometer, the Qubit 4 Fluorometer, and another supplier's single-sample fluorometer. The samples used for these assays consisted of 0.1, 1, 5, and 10 ng/µL lambda DNA for the Qubit 1X dsDNA HS Assay Kit; and 2, 20, 50, and 100 ng/µL lambda DNA for the Qubit dsDNA BR Assay Kit. Samples were run in replicates of eight in individual Invitrogen™ Qubit™ Assay Tubes (Cat. No. Q32856) on all three fluorometers. The samples were run according to the assay protocols, and the percent error and percent coefficient of variation (CV) were calculated for each sample measurement and averaged across all concentrations for each instrument.

The accuracy of quantitation (represented as % error) was assessed using the Qubit 1X dsDNA HS Assay Kit with the Qubit 4 Fluorometer, Qubit Flex Fluorometer, and another supplier's single-sample fluorometer (Figure 3A). The Qubit Flex Fluorometer was the most accurate, with an error of only 3.5%, followed by the Qubit 4 Fluorometer with a 4.5% error. The other supplier's fluorometer had lower accuracy, with a 7.9% error. Similarly, the precision of quantitation was evaluated using the Qubit dsDNA BR Assay Kit with the Qubit 4 Fluorometer, Qubit Flex Fluorometer, and another supplier's single-sample fluorometer. The CV for all samples was measured for each data point and averaged across all concentrations for each instrument. The Qubit Flex Fluorometer measurements had the lowest percent CV, indicating higher precision than the other two fluorometers tested (Figure 3B).

Improved user interface

In addition to its higher throughput, the Qubit Flex Fluorometer includes several improvements in the user interface. The instrument's user interface can be personalized to display in the language of your choice, including English, French, Spanish, Italian, German, Japanese, and simplified Chinese. Additionally, to help improve accuracy and reliability and reduce time-to-data, the Qubit Flex Fluorometer includes calculators for reagent, assay range, molarity, and normalization.

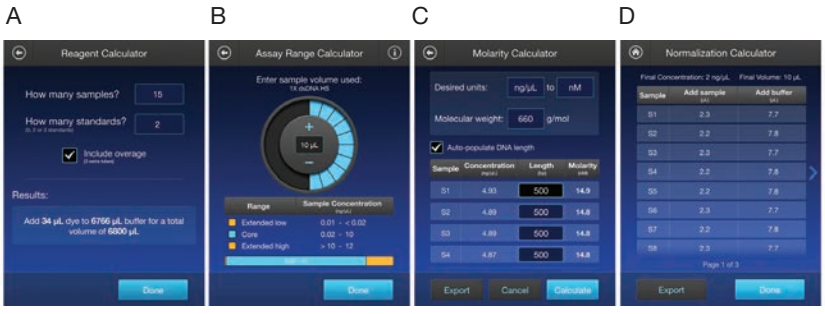

Figure 4. The Qubit Flex Fluorometer includes new calculators. (A) The Reagent Calculator helps you determine how much working solution to prepare for the number of samples. **(B)** The Assay Range Calculator displays the core sample concentration range for which the selected assay is most accurate, along with the extended low and high ranges, based on the sample volume. **(C)** The Molarity Calculator allows you to calculate the molarity of a sample based on nucleic acid length and the measured concentration. **(D)** The Normalization Calculator replaces the need to transfer the data to a spreadsheet to normalize samples during library preparation for sequencing.

The Reagent Calculator (Figure 4A) helps to determine how much working solution to prepare for the number of samples in your experiment. To help choose the best assay for the samples, the Assay Range Calculator (Figure 4B) displays the core sample concentration range for which the selected assay is most accurate, along with the extended low and high ranges, based on sample volume. To aid in various downstream applications, the Molarity Calculator (Figure 4C) allows you to calculate the molarity of a sample based on nucleic acid length and measured concentration, and the Normalization Calculator (Figure 4D) replaces the need to transfer the data to a spreadsheet to normalize samples during library preparation for sequencing. With the Normalization Calculator, the results are easily normalized to a desired mass, concentration, or molarity.

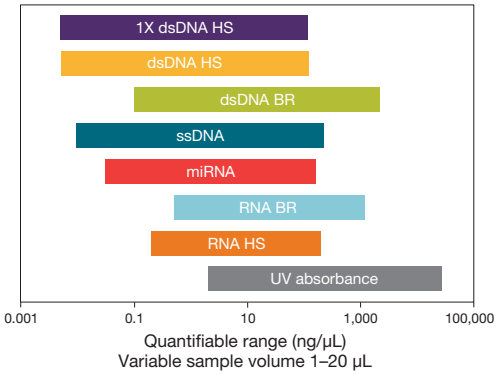

Figure 5. Comparison of sample concentration ranges for Qubit assays and UV absorbance measurements. UV absorbance readings are not selective for RNA vs. DNA. The Qubit Flex Fluorometer and Qubit assays are optimized for use together.

Exceptional selectivity and sensitivity provided by the Qubit Assay Kits

The Qubit Flex Fluorometer in combination with the Qubit assays yields analyte-specific quantitation of DNA, RNA (including miRNA), and protein over a broad concentration range and with unprecedented accuracy, sensitivity, and simplicity, for both routine analyses and rare or hard-to-obtain samples (Figure 5). The basis of each Qubit assay is a target-selective fluorescent dye that emits fluorescence only when bound to the specific target molecule, even when present at low concentrations.

The most significant advantage of the Qubit DNA and RNA assays is their selectivity. UV absorbance–based analysis cannot be used to separately quantify DNA or RNA in samples containing a mixture of both. In contrast, the Qubit DNA and RNA assays are able to accurately measure DNA and RNA, respectively, in the same sample. We found that the DNA concentration of a sample containing equal parts DNA and RNA can be measured within 2% of the actual concentration using the Qubit dsDNA BR Assay Kit. In a sample containing a 10-fold excess of RNA over DNA, the DNA concentration was measured to be only 7% higher than the actual concentration.

Each Qubit Assay Kit provides concentrated assay reagent, dilution buffer, and prediluted standards, and all assay reagents are stored at room temperature. Simply dilute the reagent using the buffer provided, add your sample (any volume between 1 and 20 µL), and read the concentration using a Qubit Fluorometer after a 2-minute incubation (allow 15 minutes for the protein assay). The Qubit assay signal is stable for 3 hours. With the Qubit Flex Fluorometer, all assay settings and calculations are performed automatically.

Bring the Qubit Flex Fluorometer to your benchtop

When laboratories need to quantify nucleic acid or protein in an increased number of samples due to changes in applications or scope of a project, a single-sample quantitation reader is not only tedious but a bottleneck in the workflow. The Qubit Flex Fluorometer is designed to address the growing need for higher-throughput DNA and RNA quantitation while maintaining all the benefits of accuracy and reproducibility that have long been associated with Qubit fluorometers and assays. The advanced optics and data analysis algorithms built into the Qubit Flex Fluorometer are optimized to work together with the Qubit assays, resulting in a seamless solution that generates highly reliable, sensitive, and specific results. To learn more or request an in-lab demonstration, visit **thermofisher.com/qubit**. ■

Product	Quantity	Cat. No.
Qubit™ Flex Fluorometer	1 fluorometer	Q33327
Qubit™ Flex NGS Starter Kit	1 kit	Q45893
Qubit™ Flex Quantitation Starter Kit	1 kit	Q45894
Qubit™ Flex Assay Tube Strips	125 tube strips	Q33252
Qubit™ Flex Assay Reservoirs	100 reservoirs	Q33253
Qubit™ 1X dsDNA HS Assay Kit	100 assays 500 assays	Q33230 Q33231
Qubit™ dsDNA BR Assay Kit	100 assays 500 assays	Q32850 Q32853
Qubit™ ssDNA Assay Kit	100 assays	Q10212
Qubit™ microRNA Assay Kit	100 assays 500 assays	Q32880 Q32881
Qubit™ RNA HS Assay Kit	100 assays 500 assays	Q32852 Q32855
Qubit™ Protein Assay Kit	100 assays 500 assays	Q33211 Q33212

The effects of inflammation on the mutational spectrum of clonal hematopoiesis of indeterminate potential (CHIP)

Inflammatory cytokines promote clonal hematopoiesis with specific mutations in ulcerative colitis patients.

Zhang CRC, Nix D, Gregory M, Ciorba MA, Ostrander EL, Newberry RD, Spencer DH, Challen GA (2019) *Exp Hematol* 80:36–41.

The aging-related premalignant condition known as clonal hematopoiesis of indeterminate potential (CHIP) is characterized by a distinct subset of hematopoietic stem cells (HSCs) carrying one or more somatic mutations, typically in myeloid malignancy–associated genes. This subset of HSCs produces a clonal population of blood cells that can be identified in blood samples from individuals before symptoms are ever present (in ~10% of people over 65 years old). Even with CHIP, most of these individuals are at low risk of acquiring a hematologic malignancy.

In their recent *Experimental Hematology* paper, Zhang and colleagues investigated the role of environmental factors, specifically inflammation, on the mutational spectrum of CHIP blood cell subpopulations. They postulated that in addition to compromising HSC function, an inflammatory environment may also exert selective pressure on HSC mutations associated with CHIP. In their study, they sequenced 40 CHIP-associated genes in the peripheral blood mononuclear cell DNA from 187 patients >50 years old with ulcerative colitis (UC). UC is an inflammatory bowel disease that leads to T cell infiltration of the colon, as well as the overproduction of two pro-inflammatory cytokines, tumor necrosis factor α (TNFα) and interferon γ (IFNγ). They found that the most frequently mutated gene in those UC patients with CHIP was *DNMT3A*, followed by *PPM1D*, suggesting that inflammation associated with UC may exert selective pressure on the CHIP mutational spectrum.

In addition to analyzing DNA sequences, Zhang and coauthors quantified patient TNFα and IFNγ levels using the corresponding Invitrogen™ ProQuantum™ Immunoassay Kit, which provides a sensitive qPCR-based immunoassay that can detect as little as 0.01 pg/mL cytokine in serum using small sample volumes. The pro-inflammatory cytokine data from the UC patients were matched for patient age and sex, and further grouped into three categories: CHIP$^-$ (n = 21), CHIP-hs$^+$ (CHIP-high sensitivity with variant allele fraction >0.5%) without *DNMT3A* mutations (CH$^+$*DNMT3A*$^-$, n = 17), and CHIP-hs$^+$ with *DNMT3A* mutations (CH$^+$*DNMT3A*$^+$, n = 19). Whereas serum TNFα levels were not significantly different among patient groups, the CHIP-hs$^+$ CH$^+$*DNMT3A*$^+$ patients exhibited significantly higher serum IFNγ levels (Figure 1).

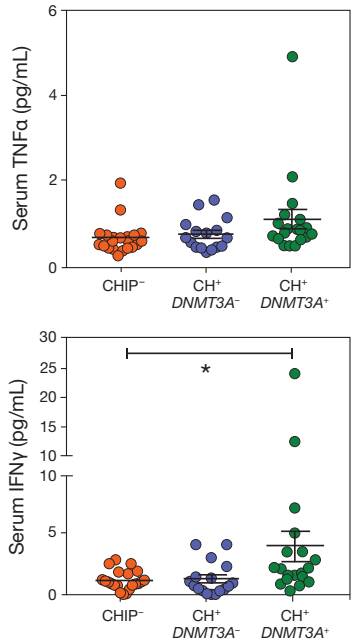

Figure 1. Clonal hematopoiesis of indeterminate potential (CHIP) dynamics in ulcerative colitis (UC) patients. TNFα and IFNγ levels in serum of UC samples in patients surveyed in this experiment, measured using Invitrogen™ ProQuantum™ Immunoassay Kits. Each dot indicates the level of a given cytokine in the serum of one patient. Graphs represent means ± SEM. * $p < 0.05$, one-way ANOVA with Bonferroni multiple test correction. Reprinted from Zhang CRC, Nix D, Gregory M et al. (2019) *J Exp Hematol* 80:36–41, with permission from Elsevier.

In summary, this study showed that UC patients were slightly more likely to have CHIP, and that inflammation associated with UC may be selecting for HSC clones with specific mutations. Further research is needed to explore the relationship between IFNγ levels and *DNMT3A* mutations. ■

Product	Quantity	Cat. No.
ProQuantum™ Human IFNγ Immunoassay Kit	96 tests 5 x 96 tests	A35576 A355765
ProQuantum™ Human TNFα Immunoassay Kit	96 tests 5 x 96 tests	A35601 A356015

For more information and to see the full selection of Invitrogen™ ProQuantum™ Immunoassay Kits, go to **thermofisher.com/proquantum**.

Cover image

Fluorescence imaging of a labeled macrophage. Monocytes were isolated from human peripheral blood mononuclear cells (PBMCs) using Invitrogen™ Dynabeads™ Untouched™ Human Monocytes Kit (Cat. No. 11350D), then differentiated into macrophages for 7 days in Gibco™ RPMI 1640 Medium (Cat. No. 11875168) with 10% Gibco™ Fetal Bovine Serum (Cat. No. 26140087), 8% human serum, 1% Gibco™ GlutaMAX™ Supplement (Cat. No. 35050061), 20 mM HEPES, 1% Gibco™ Penicillin-Streptomycin (10,000 U/mL, Cat. No. 15140122), and 50 ng/mL Gibco™ M-CSF Recombinant Human Protein (Cat. No. PHC9501). Macrophages prepared in this manner are useful models for studying antibody-dependent phagocytosis of cancer cells or phagocytosis of microorganisms. These human monocyte–derived macrophages were cultured in a 96-well microplate before labeling with Invitrogen™ CellTrace™ Violet dye (pseudocolored red, Cat. No. C34557), which labels the entire cell but the cell body most intensely, and a fluorescent live-cell actin tracking stain (pseudocolored purple). This labeled macrophage (~50 µm in diameter) was imaged using the Invitrogen™ EVOS™ M7000 Imaging System (Cat. No. AMF7000) with an Olympus™ 60x apochromat oil objective (Cat. No. AMEP4694).

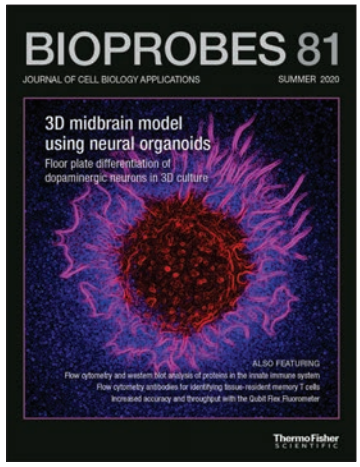

Previous issues

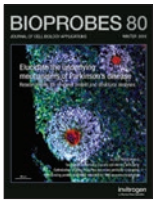

BIOPROBES 80

This issue focuses on fixed- and live-cell tools for the advancement of Parkinson's disease research, including antibodies and fluorescent tubulin stains. Also described are complementary immune-cell phenotyping assays, RNA-binding protein antibodies, and Invitrogen™ Alexa Fluor™ Plus secondary antibodies. In addition, we report the use of Invitrogen™ CellEvent™ Senescence Green Probe for drug discovery research.

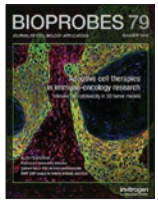

BIOPROBES 79

This issue features adoptive cell therapies in immuno-oncology research and the use of cytotoxicity assays with 3D tumor models. Also discussed are best practices for multiparameter flow cytometry, antibodies and immunoassays for signaling pathway research, and functional assays for senescence, drug-induced calcium flux, microtubule dynamics, and biofilm cell viability.

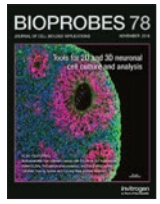

BIOPROBES 78

In this issue, we describe media, cultureware, and reagents for 2D and 3D neuronal cell culture and fluorescence imaging, as well as time-saving immunoassays such as Invitrogen™ Instant ELISA™ kits, ProQuantum™ kits, and ProcartaPlex™ multiplex panels. We also highlight the Thermo Scientific™ Multiskan™ Sky Microplate Spectrophotometer and the Invitrogen™ Attune™ NxT Autosampler for high-throughput assays.

Back issues of *BioProbes Journal* published after 1995 are available at **thermofisher.com/bioprobes**. Subscribe to *BioProbes Journal* at **thermofisher.com/subscribebp**.

Thermo Fisher Scientific

5781 Van Allen Way
Carlsbad, California 92008
United States
Tel: +1 760 603 7200
Toll-Free Tel: 800 955 6288
Fax: +1 760 603 7229
Email: techsupport@thermofisher.com

APEX 30 YEARS 1988 2018 AWARDS FOR PUBLICATION EXCELLENCE

For Research Use Only. Not for use in diagnostic procedures.

COL011872 0520

thermofisher.com/bioprobes

ThermoFisher SCIENTIFIC